Multisensory gamma stimulation enhances adult neurogenesis and improves cognitive function in male mice with Down Syndrome

Md Rezaul Islam*[1,2], Brennan Jackson*[1,2,3], Maeesha Tasnim Naomi[1,2], Brooke Schatz[1,2], Noah Tan[1,2], Mitchell Murdock[1,2], Dong Shin Park[1,2], Daniela Rodrigues Amorim[1,2], Fred Jiang[4], S. Sebastian Pineda[1,5,6], Chinnakkaruppan Adaikkan[1,2], Vanesa Fernandez[1,2], Ute Geigenmuller[1,2], Rosalind Mott Firenze[1,2], Manolis Kellis[5,6], Edward S. Boyden[4,7,8], Li-Huei Tsai[1,2,6#]

Affiliations
[1]Picower Institute for Learning and Memory, Massachusetts Institute of Technology, Cambridge, MA, USA.
[2]Department of Brain and Cognitive Sciences, Massachusetts Institute of Technology, Cambridge, MA, USA.
[3]Institute for Medical Engineering and Science, Massachusetts Institute of Technology, Cambridge, MA, USA.
[4]Departments of Biological Engineering and Brain and Cognitive Sciences, McGovern Institute, Cambridge, MA, USA.
[5]MIT Computer Science and Artificial Intelligence Laboratory, Cambridge, MA, USA.
[6]Broad Institute of MIT and Harvard, Cambridge, MA, USA.
[7]Koch Institute, Massachusetts Institute of Technology, Cambridge, MA, USA.
[8]Howard Hughes Medical Institute, Massachusetts Institute of Technology, Cambridge, MA, USA.

*Equal contribution
#Corresponding author; Li-Huei Tsai, PhD; E-mail: lhtsai@mit.edu

Summary

Down syndrome (DS) has been linked with deficits in hippocampal dependent cognitive tasks and adult neurogenesis, yet treatment options are still very limited. We and others previously showed that a non-invasive multisensory gamma stimulation using light and sound at 40 Hz ameliorated Alzheimer's disease pathology and symptoms in mouse models. In this study, we tested the effects of 40 Hz multisensory stimulation in the Ts65Dn mice, a mouse model of DS. For three weeks, mice were exposed daily to one hour of stimulation or one hour of ambient light and sound. Mice receiving the stimulation showed improved object recognition and spatial working memory. Using single nuclei RNA-seq and experimental validations in mouse hippocampal samples, we identified underlying expression changes in gene regulatory networks and demonstrated increased adult neurogenesis and reorganization of synapses as potential mechanisms for these improved cognitive phenotypes. Together, our data reveal a novel effect of multisensory gamma stimulation on adult neurogenesis and beneficial effects of 40 Hz treatment on cognitive function in DS model mice.

Keywords: Multisensory gamma stimulation; 40 Hz; single nuclei RNA-seq; gene-regulatory network; Down syndrome; non-invasive therapy

Significance Statement

We present strong evidence, using a well-characterized mouse model, that the cognitive and neurogenesis deficits in Down syndrome can be improved through non-invasive multi-sensory gamma stimulation. Employing a systems biology approach, we provide extensive hippocampal single-cell resolution gene expression signatures and changes in gene regulatory networks in response to sensory gamma stimulation.

Main Text

Introduction

Down syndrome (DS) has been linked with impaired neurogenesis [1] and aberrant synaptic functions in the hippocampus [2]. These changes are consistent with the reported deficits in memory and other cognitive tasks in individuals with DS [3,4]. Additionally, a recent study found dementia to be associated with mortality in 70% of older adults with DS [5]. However, there are currently limited therapeutic options available to manage cognitive performance in individuals with DS. We have previously reported the utility of using sensory stimulation presented at gamma frequency for combating cognitive decline in mouse and human subjects [6–8]. The sensory gamma stimulation reduced Alzheimer's disease (AD) related pathology, improved neuronal survival and synaptic density, and enhanced cognitive function in multiple mouse models of AD [7,9,10]. In a more recent literature, we showed that the reduced pathology was specifically observed at 40 Hz stimulation but not at 8 or 80 Hz stimulation [9]. Others have also reported the beneficial effects associated with gamma stimulation in AD [11–13] as well as in other neurological diseases such as Parkinson´s disease [14]. However, the efficacy of sensory gamma stimulation at 40Hz has not been tested in DS. The Ts65Dn mouse, the most widely used model of DS, contains an extra chromosome spanning most of the distal region of mouse chromosome 16 homologous to human chromosome 21 [15]. This murine model recapitulates phenotypes present in individuals with DS including synaptic abnormalities [16] and deficits in hippocampal-dependent spatial learning and memory [15]. As such, this murine model provides invaluable opportunities for exploring and testing potential therapeutic interventions for cognitive deficits in DS. Here, we used this well-characterized DS mouse model to test the effects of sensory gamma stimulation on cognitive benefits within the DS model and observed that this treatment improved cognitive function, enhanced adult neurogenesis, and induced expression changes in genes involved in synaptic organization.

Results

Multisensory gamma stimulation improves cognitive performance of Ts65Dn mice

To examine the effect of the sensory gamma stimulation on cognitive performance in DS, we used the Ts65Dn mouse model of DS, which recapitulates phenotypes present in individuals with DS including synaptic abnormalities [16] and deficits in hippocampal-dependent spatial learning and memory [15] and adult neurogenesis [17]. We exposed one group of Ts65Dn mice to one hour of 40 Hz auditory and visual stimulation per day (stimulation), while a parallel group was exposed to ambient light and sound (ambient, **Fig 1A**). Littermate wild-type controls were not included in this experimental setup since the well-established cognitive deficits of Ts65Dn mice in hippocampus-dependent tasks, as reported in previous studies [15,18,19], offer a clear benchmark for evaluating the effects of stimulation on cognitive improvements. Shortly before the completion of the three-

85 week treatment period using the 40 Hz or ambient auditory and visual stimulation, we conducted
86 the Novel Object Recognition (NOR), Novel Object Location (NOL), and elevated Y-maze
87 behavioral tests to evaluate the effects of the stimulation on object recognition (**Fig 1B**) and spatial
88 memory (**Fig 1C-D**). For the NOR/NOL tests, both groups of mice were first presented with two
89 objects in fixed locations. When one of the familiar objects was later replaced by a novel object in
90 the same location (NOR, **Fig 1B**) or placed in a novel location (NOL, **Fig 1C**), the stimulation
91 group spent a significantly higher percentage of time than the ambient group exploring the novel
92 object (stimulation = 64.1+/-12.3%, ambient = 48.6+/-21.5%, $p = 0.04$) and the familiar object in
93 the novel location (stimulation = 73.4+/-11.7% vs ambient = 46.6+/-15.4%, $p < 0.001$).
94 Importantly, the observed changes in performance between stimulation and ambient groups were
95 not related to differences in locomotory behaviors in an open field area (**Fig S1A, Fig S1B**). Thus,
96 the NOR/NOL results indicate a clear improvement in both object recognition and spatial memory
97 in the stimulation group compared to the ambient group. Spatial memory was further assessed by
98 spontaneous alternation in the elevated Y-maze test, which allows mice to freely explore the three
99 arms of a Y-shaped maze. Consecutive entries into three different arms are considered a
100 spontaneous alternation, expressed as % of all possible entry triads. Mice with stimulation
101 demonstrated a significantly higher number of spontaneous alternations than the ambient group
102 (stimulation = 61.15+/-9.1%, ambient = 51.3+/-8.7%, $p = 0.02$, **Fig 1D**), while the number of total
103 entries was not significantly different between the two groups (stimulation = 29.2+/-7.9, ambient
104 = 24.1+/-6.3, **Fig 1D**). These results indicate improved spatial working memory in DS mice in
105 response to stimulation. Since both object recognition and spatial memory are hippocampus-
106 dependent memory tasks, the behavioral testing results also imply that the sensory stimulation
107 impacts hippocampal neurons. This was experimentally confirmed by performing staining for c-
108 Fos, a widely used marker of neuronal activity [20], on brain sections from mice in the stimulation
109 and ambient groups. Mice in the stimulation group showed an increased proportion of c-Fos
110 positive nuclei in the hippocampus compared to mice in the ambient group (**Fig S2**).
111
112 **Multisensory gamma stimulation increases expression of synapse-related genes in excitatory**
113 **neurons in the hippocampus of Ts65Dn mice**
114
115 To decipher potential mechanisms underlying sensory stimulation-mediated cognitive
116 improvement in Ts65Dn mice, we performed single-nucleus RNA sequencing (snRNA-seq) on
117 hippocampal samples from the stimulated and ambient groups of mice (**Fig 2A)**, yielding 15,884
118 nuclei with high quality transcriptomic profiles (**Fig S3**). Based on the top variable genes, the
119 nuclei were categorized into transcriptionally distinct clusters that could be visualized in uniform
120 manifold approximation and projection (UMAP) space and assigned to principal brain cell types
121 based on the expression of canonical markers (**Fig 2B, Fig S3E**). The majority (69.7%) of captured
122 nuclei represented neurons (54.5% excitatory and 15.2% inhibitory), 26.5% were derived from
123 glial cells, and the remaining 3.8% represented vascular and choroid plexus cells (**Fig S3F**).

Samples were well integrated across both groups (**Fig S3G**), and broad cell type constituency did not differ significantly between the stimulation and ambient groups (**Fig S3H)**.

We then performed differential gene expression analyses focusing on the neuronal clusters. Excitatory neurons showed a higher number of gene expression changes in response to the stimulation than inhibitory neurons, with 108 genes upregulated and 104 genes downregulated in the stimulation group compared to the ambient group (**Fig 2C**, **Fig S3I**, **Table S1**). Using a curated list of synaptic genes as reference [21], we found that synaptic genes were significantly overrepresented within the set of 108 upregulated genes (Fisher's exact test, p value = 0.004; **Table S2**). Differentially upregulated synaptic genes included *Actb, Actg1, Atp6voc, Camk2b, Frrs1l, Gphn, Gpm6a, Hspa8, Il1rapl1, Mdga2, Nptn, Nrg1, Rab14, Rock1, Syt11*, and *Tuba1a*, of which several have been implicated in synaptic functions [22], synapse development [23], or synaptic plasticity [24]. Gene ontology (GO) analyses further demonstrated that the genes differentially expressed in excitatory neurons in response to stimulation were associated with various synaptic functions, with the majority related to synapse organization (e.g., synaptic vesicle endocytosis, synapse assembly, synapse organization, post-synapse organization, regulation of synapse organization, and regulation of synapse structure) (**Fig 2D**), and that some of these processes were also altered in inhibitory neurons (**Fig 2D**). Of note, reanalysis of published datasets (see Methods) unveiled downregulation of synapse organization associated genes in the brains of Ts65Dn mice (**Fig S4A-B, Table S3**) as well as in excitatory neurons in individuals with DS (**Fig S4C, Table S3**) compared to healthy controls.

To strengthen these findings in excitatory neurons and for additional insights, we employed an orthogonal computational approach. Using a weighted gene co-expression analysis (WGCNA), we identified seven gene regulatory modules in hippocampal excitatory neurons (**Fig 2E, Table S4, Fig S5A-B**). Three of these seven gene modules (Ex-3, Ex-6, Ex-7) showed significantly increased expression in the stimulation group compared to the ambient group, two (Ex-1 and Ex-2) displayed decreased expression (**Fig 2E**, **Fig S5C**), and two (Ex-4, Ex-5) showed no expression changes (**Fig 2E**). Focusing our downstream analyses on the three upregulated gene modules, we found that several of the hub genes encode synaptic proteins (**Fig 2F**) and few of these genes are implicated in synaptic organization (Farp1 [25]), synapse formation (Ptprt [26]) and synapse development (Lrrc4c [27], Efna5 [28]). Therefore, increased expression of these three gene modules may alter functional synapses in the hippocampus of the stimulation group.

To test this hypothesis experimentally, we performed immunostaining for the post-synaptic marker PSD95 and the pre-synaptic marker synaptophysin in the granule cell molecular layer of the dentate gyrus in the hippocampi from the ambient and stimulation groups (**Fig 2H**). Co-localization of both markers served as the readout of putative synapses. The stimulation group showed a significant increase in the number of such putative synapses in the dentate gyrus (**Fig 2H**), while no significant increase in the number of such synapses was seen in the CA1 region of the hippocampus (**Fig S6**). These findings confirm that the gene expression changes observed in

164 response to stimulation lead to region-specific modification in synaptic organization within the
165 hippocampus.

166 To better understand the molecular mechanisms, we focused on gene co-expression analyses rather
167 than differential expression analyses for downstream analyses. Gene co-expression analyses
168 enable the investigation of gene expression changes in a systems level framework [29]. Moreover,
169 such analyses have potential to identify gene regulatory networks underlying complex biological
170 phenotypes [30]. Additionally, they allow for comparative data analyses with existing datasets;
171 and the hub genes identified based on co-expression analyses are potentially the driver of the gene
172 circuits and provide critical insights into the underlying biological mechanisms [31,32]. Further
173 analyses of the gene modules unveiled several hub genes that are associated with Alzheimer´s
174 Disease (AD) related dementia (**Fig 2I)**. Among those, *Reln* in particular has been implicated in
175 AD [33,34] and aging [35], and a gain-of-function variant in this gene has been shown to confer
176 resilience against autosomal dominant AD [36]. Remarkably, IHC unveiled an increased
177 proportion of *Reln*+ neurons in the CA3 (**Fig 2J**) and DG (**Fig S7**) regions but not in the CA1
178 region (**Fig S7**) of the hippocampus of our stimulation group compared to the ambient group (**Fig
179 2J**).
180
181 Based on these observations and to further validate the significance of the three gene modules in
182 cognitive benefits, we examined their expression patterns in published transcriptomic datasets (see
183 Methods) focusing on aging and AD, both known risk factors for cognitive decline. Interestingly,
184 we observed reverse expression pattern of these gene modules in context to the cognitive decline.
185 Specifically, all three modules showed a steady decrease in expression with increasing age (**Fig
186 S8**). In line with this, the gene modules particularly module Ex-3 and Ex-7 (both increased after
187 stimulation), significantly overlapped with genes downregulated in excitatory neurons with aging
188 (**Fig 2K, Table S5**) or AD (**Fig 2L, Table S6**) in mice and humans. Together, these data further
189 confirm that gamma stimulation can increase expression of cognitively relevant gene modules in
190 excitatory neurons and thus potentially contribute to the observed cognitive benefits.
191
192
193 **Multisensory gamma stimulation increases adult neurogenesis in Ts65Dn mice**
194 Since the Ex-7 (61 genes) module most consistently displayed overlap across aging and AD
195 datasets in both mouse and humans (Fig 2K, 2L), we analyzed the transcription factors (TFs) for
196 this module to identify upstream regulators. Among the TFs whose targets overlap with the module
197 genes, TCF4 emerged as the highest ranked transcription factor when using a p value based on a
198 hypergeometric test (**Fig 3A**, **Table S7**). Additionally, predicted TCF4 targets such as Nrg1, Rfx7,
199 Robo2, Ttc3 were upregulated in excitatory neurons based on the differential expression analysis
200 (**Table S1A**). This finding suggests that the differential gene expression and gene co-expression
201 analyses converge on a common upstream gene regulatory factor. Interestingly, TCF4 is critical
202 for progenitor proliferation [37], the peak of TCF4 expression coincides with neurogenesis [38],
203 and it regulates neurogenesis and neuronal migration [39]. Moreover, TCF4 is a critical regulator

204 that facilitates adult neurogenesis [40], and deficits in TCF4 expression lead to impaired adult
205 hippocampal neurogenesis in mice [41]. Thus, we focused on TCF4 expression in the dentate gyrus
206 of the hippocampus, a brain region that has been linked to adult neurogenesis. Excitingly, we
207 observed dentate gyrus-specific increased TCF4 expression in the Ts65Dn mice after gamma
208 stimulation (**Fig 3B, Fig S9**). Thus, we hypothesized that the stimulation might have an impact on
209 adult neurogenesis.

210 Previous studies have leveraged snRNA-seq datasets, specifically the transcriptional profile of
211 granule cells (GCs), to address adult neurogenesis in mice [42] and in humans [43]. To investigate
212 whether gamma stimulation can affect adult neurogenesis, we sorted nuclei based on the
213 expression of Prox1, a pan-GC marker [42,44], and selected GC using an *in silico* approach
214 (Materials and Methods, **Fig S10**). We ordered cells along the GC developmental trajectory (**Fig**
215 **S11**), identified genes whose expression changed as a function of pseudotime (**Fig S11A**), and
216 then analyzed the effect of gamma stimulation on gene expression changes along this GC
217 developmental trajectory (**Table S8**). GO analysis revealed that 40 Hz stimulation induced
218 differential expression of genes related to biological processes of various themes related to adult
219 neurogenesis (e.g., neuron projection development, synapse organization, regulation of RNA
220 splicing, microtubule-based transport, and cell morphogenesis involved in neuron differentiation)
221 (**Fig S11B**) and that some of these processes overlapped with those reported to be downregulated
222 in immature GCs in aging [43]. When analyzing immature granule cells (GCs) in this study, as
223 further confirmed by the expression of immature GC markers (**Fig S10**), we detected three distinct
224 subclusters (**Fig 3C**). Each subcluster was characterized by the expression of specific marker genes
225 that differentiated it from the others (**Fig 3D**). Among these clusters, cluster 3 was transcriptionally
226 distinct from the other two clusters (**Table S9**), with its differentially expressed genes associated
227 with adult neurogenesis-related biological processes (e.g., neuron migration, regulation of
228 neurogenesis, oxidative phosphorylation, and cellular respiration) (**FigS11C)**. Intriguingly, the
229 proportion of cluster 3 was significantly increased in the stimulation group (**Fig 3E-F)** compared
230 to the ambient group**,** suggesting a potential increase in neurogenesis.

231 To experimentally validate the impact of gamma stimulation on adult neurogenesis, we adopted
232 two different experimental approaches for directly testing for cell proliferation in the dentate gyrus.
233 In the first approach, fixed brain slices from both the stimulation and ambient groups were stained
234 for Ki67, a marker for cellular proliferation (**Fig 3G**). The stimulation group exhibited a
235 significantly higher number of Ki67+ cells in the sub-granular zone of the dentate gyrus compared
236 to ambient group (stimulation = 18.3+/-1.3, ambient = 12.0+/-4.4, p = 0.027, **Fig 3G**), suggesting
237 increased neurogenesis. In the second approach, a separate cohort of stimulation and ambient
238 Ts65Dn mice were injected with EdU (25 mg/kg), a nucleoside analog of thymidine that labels
239 newly synthesized DNA and thus proliferating cells, for 2 days prior to perfusion (**Fig 3H)**. In this
240 cohort, mice in the stimulation group showed a significant increase in the number of cells positive
241 for EdU in the dentate gyrus (stimulation = 8.1+/-3.1, ambient = 4.5+/-2.9, p = 0.03, **Fig 3H**),
242 again indicating that 40 Hz sensory stimulation increased adult neurogenesis in TsD65n mice.

Together, our results demonstrate that 40Hz stimulation can increase adult neurogenesis and improve cognitive performance in the Ts65Dn mouse model. Furthermore, our findings suggest that these improvements are related to changes in the expression of hippocampal gene regulatory networks that are involved in synaptic organization within the hippocampus and show association with aging and AD and to enhanced adult neurogenesis.

Discussion

In this study, we investigated the efficacy of a non-invasive multisensory gamma stimulation to improve cognitive functions in male Ts65Dn mice, a widely used mouse model of DS, at 6-8 months of age. The Ts65Dn mice at that age do not exhibit increased levels of APP in the hippocampus [45] and lack the insoluble amyloid plaques and neurofibrillary tangles characteristic of AD [15,46], but do show some early symptoms of AD-related pathologies such as increased levels of soluble amyloid Aß40 and Aß42 in the hippocampus [47], signs of hippocampal-dependent cognitive impairments [46,48], and hippocampal degeneration [49]. Since approximately 90% of adults with DS will develop AD in their lifetimes and show substantial Aß accumulation and NFTs in the brain by age 40 [50], as well as increased soluble Aß in the brain [51], the presence of some AD-like features in Ts65Dn mice makes this model particularly suitable for studying early AD pathology in DS and testing the therapeutic potential of multisensory gamma stimulation. Our study reveals beneficial effects of multisensory gamma stimulation on cognitive performance in hippocampal-dependent tasks and on adult neurogenesis and provides hippocampal gene expression signatures and gene regulatory networks at the single cell resolution. We show that three weeks of daily one-hour multisensory stimulation improved spatial memory and object recognition in Ts65Dn mice. Importantly, these changes were not confounded by locomotory behaviors, suggesting gamma stimulation-specific effects on hippocampal-dependent memory and recognition, which is consistent with previous observations in mouse models of AD and neurodegeneration [6,7].

The specific impact of the sensory gamma stimulation on transcriptomic changes and gene regulatory network within the hippocampus, particularly at the single cell level, has not previously been investigated. Here, we used snRNA-seq of hippocampal tissue from Ts65Dn mice to describe the hippocampal molecular signatures underlying the spatial cognitive benefits from sensory gamma stimulation. We showed that the stimulation increased expression of genes related to synapse organization in excitatory neurons. Moreover, we identified specific gene regulatory modules upregulated by 40 Hz stimulation within the excitatory neurons that significantly overlap with genes downregulated during aging and in AD. This finding further highlights the relevance of these gene modules for cognitive benefits. Sensory-evoked modulation of these genes are particularly intriguing given that early clinical studies have shown sensory 40 Hz stimulation – which is non-invasive, inexpensive, and easily administered in a home setting – to be safe and tolerable in humans [11]. Several of the hub genes in the gene modules with increased expression after the sensory treatment have been implicated in learning and memory, general cognitive

283 function, and/or AD based on GWAS studies, such as *Adcy8*, *Gria4* or *Reln*. A potential role of
284 Reelin in providing cognitive benefits in DS mice is further supported by experimental
285 confirmation. In our previous work, where we identified *Reln*+ neurons as particularly vulnerable
286 in AD [52]. Excitingly, in this study, sensory gamma stimulation increased the number of *Reln*+
287 neurons in the hippocampus in a subregion-specific manner. Given that DS is a significant risk
288 factor for AD in humans, these findings in the Ts65Dn mouse model are particularly intriguing, as
289 the genes with altered expression following 40 Hz stimulation overlap with those implicated in
290 AD, providing potential avenues for treating AD pathologies in DS.
291
292 We further identified *TCF4*, a critical factor in adult neurogenesis [40,41], as one of the upstream
293 regulators for the most conserved gene module and not only observed a notable increase in *TCF4*
294 expression specifically in the dentate gyrus after 40 Hz stimulation, but directly demonstrated an
295 increase in adult neurogenesis in the dentate gyrus of Ts65Dn mice. Although the exact role of
296 adult hippocampal neurogenesis on memory continues to be elucidated, extensive evidence has
297 shown its connection to hippocampus dependent tasks both under conditions that deplete
298 neurogenesis [53] as well as conditions that promote neurogenesis (e.g., genetic [54] or
299 pharmacological [55] interventions, exercise [56], and environmental enrichment [57]). In Ts65Dn
300 mice, specifically, interventions that rescue neurogenesis have been shown to lead to
301 improvements in novel object recognition and novel object location [58–61].
302
303 Additionally, we noted that 40 Hz stimulation increased expression of genes related to synaptic
304 organization and the number of putative synapses, as identified by co-localization of PSD95 puncta
305 with pre-synaptic synaptophysin puncta, in the dentate gyrus. It is likely that these hippocampal
306 synaptic changes along with increased neurogenesis underlie the improved hippocampal-
307 dependent tasks in 40Hz stimulation.
308
309 The present study reveals a beneficial impact of three-week long 40 Hz multisensory gamma
310 stimulation of adult Ts65Dn male mice on their cognitive performance, neurogenesis, and
311 hippocampal synaptic organization highlighting the potential of gamma stimulation as a
312 therapeutic strategy for cognitive deficits in individuals with DS. Of note, one limitation of this
313 study is that the Ts65Dn mice display trisomy for only approximately two-thirds of the genes
314 orthologous to human chromosome 21 (Hsa21), but also for some genes that are not triplicated in
315 human DS, including ~35 protein-coding genes arising from mouse chromosome 17 (Mmu17)
316 [62,63]. Although the chronic multisensory gamma stimulation did not cause expression changes
317 for these genes, this additional triplication may introduce phenotypic effects unrelated to DS,
318 potentially confounding the interpretation of results specific to DS-related pathology. Further, the
319 transmission of the trisomy is carried through the maternal germline, requiring that the mothers be
320 trisomic, which is generally not the case in humans. Thus, findings in this study should ideally be
321 validated in other alternative DS mouse models [63]. Another limitation is that the study focused
322 solely on hippocampal gene expression changes, even though the prefrontal cortex is a critical

323 brain region involved in spatial memory, particularly for the alternation tests performed in this
324 study. Thus, future research should also investigate the effects on the gene expression changes in
325 the prefrontal cortex. Furthermore, the current study examined the effects of gamma stimulation
326 at 40 Hz exclusively in male mice, highlighting the need for future studies to include both sexes
327 and test other frequencies. Such studies will provide a more comprehensive understanding of the
328 beneficial effects of the multisensory gamma stimulation and to explore potential of its sex-specific
329 effects on cognitive performance [64], hyperactivity [15,65], developmental milestones [66] and
330 soluble amyloid pathology (e.g., Aß40, Aß42) [47] in Ts65Dn mouse model. Additionally, the
331 current study assessed only the short-term memory effects of multisensory gamma stimulation.
332 Future studies should explore its impact on long-term memory, investigate whether multimodal
333 sensory integration is critical for cognitive benefits and assess if treatment benefits can be further
334 increased by longer durations of multisensory 40 Hz treatment and/or earlier treatment onset, such
335 as in the early post-natal stage, or addition of other sensory modalities (e.g., tactile stimulation
336 [67]).
337

338 ## Materials and Methods

339 **Animals**
340 All animal work was approved by the Committee for Animal Care of the Division of Comparative
341 Medicine at the Massachusetts Institute of Technology and by the Institutional Animal Care (MIT-
342 CAC, approval number: 0621-033-24). Male Ts65Dn mice aged 6-8 months were used for all
343 experiments. Mice were housed in groups no larger than five on a standard 12-h light/12-h dark
344 cycle; all experiments were performed during the light cycle. Food and water were provided
345 without restriction. For all experiments, mice from the same litter were divided into different
346 conditions, respectfully. If additional groups were added, respective ambient groups were always
347 repeated concurrently. For tissue collection, mice were anesthetized with isoflurane and cardiac
348 perfused with ice cold DPBS (Thermo Fisher Scientific, 14190235).
349

350 **Concurrent 40 Hz auditory and visual stimulation protocol**
351 Light flicker stimulation was delivered as previously described [10,68]. Mice were transported
352 from the holding room to a separate stimulation room, located on another floor. Mice were
353 habituated under dim light for 30 min before the start of the experiment, and then introduced to
354 the stimulation cage (like the home cage, except without bedding and three of its sides covered
355 with black sheeting). All sensory gamma stimulation protocols were administered daily for 1h/d
356 for the number of days as specified. Mice were exposed to one of two stimulations: dark/quiet or
357 concurrent 40 Hz light flicker and auditory tone for one hour per day. Mice were allowed to freely
358 move inside the cage but did not have access to food or water during the 1-hour stimulation period.
359 An array of light emitting diodes (LEDs) was present on the open side of the cage and was driven
360 to flicker at a frequency of 40 Hz with a square wave current pattern and 50% duty cycle using an

Arduino system. The luminescence intensity of light that covered inside the total area of multisensory stimulation cage varied from ~ 200 – 1000 lux as measured from the back and front of the cage (mice were free to move in the cage). For audio stimulation, a 10 kHz tone at 60 dB was played at 40 Hz with a 4% duty cycle from a speaker located above the stimulation cages. After 1h of stimulation, mice were returned to their home cage and allowed to rest for a further 30 min before being transported back to the holding room. Ambient mice group underwent the same transport and were exposed to similar cages with similar food and water restriction in the same room but experienced only normal room light and natural environmental noise for the 1h duration.

Behavior

Behavioral protocols were conducted towards the end of the 3-weeks stimulation protocol. Ethanol was used to wipe down all testing apparatuses between uses.

Novel Object Recognition

The novel object recognition (NOR) task consisted of a habituation phase followed by training and testing performed the following day, as previously described [69]. 24 hours before training, mice were habituated to an open testing arena (40 cm L x 40 cm W x 35 cm H) for 10 min, during which total distance (cm), time in the center (s), and velocity (cm/s) were calculated (TSE Systems) to evaluate open field behavior. During training, mice were placed into the same box with two identical objects placed in opposite corners. Mice were allowed a total of 20 s of object interaction time (within a maximum time frame of 10 minutes), and then immediately removed from the arena. Object memory was tested 1 hour later using the same procedure during training, except one object was replaced with a novel one in its place. Object exploration was recorded when the snout contacted either object and was calculated by a recognition index, RI = (Tnovel/(Tnovel+Tfamiliar)) x100, where Tnovel and Tfamiliar indicate the time spent with the novel and familiar object, respectively.

Novel Object Location

The novel location recognition (NOL) task was performed using the same procedure as the object recognition task, except two identical objects were used for both training and testing, and one object was displaced to a novel location during testing.

Spontaneous Alternation

A Y-maze was used for testing with an apparatus with three equal arms (30 cm length, 10 cm width, and 20 cm height) placed 120° apart, made of opaque acrylic glass. A mouse was placed at the maze center and was allowed 7-min of exploration of the environment. An arm entry was scored when the mouse entered the arm with all four paws. Total number of entries (N) and number of ‘correct’ triplets (M, consecutive choices of each of the three arms without re-entries) was evaluated. The alternation rate was computed according to the formula: R (%)=(M/(N-2))x100.

401 **Single-nucleus RNA sequencing**
402 24 hours after the final stimulation session, the hippocampi of the mice were dissected and snap
403 frozen in liquid nitrogen and stored at −80 °C. The protocol for the isolation of nuclei from frozen
404 brain tissue was adapted from a previous study [70]. All procedures were carried out on ice.
405 Briefly, two mouse hippocampi were pooled per sample (3 samples per condition) and
406 homogenized in 1 ml homogenization buffer (320 mM sucrose, 5 mM CaCl2, 3 mM Mg
407 (CH3COO)2, 10 mM Tris HCl pH 7.8, 0.1 mM EDTA pH 8.0, 0.1% IGEPAL CA-630, 1 mM β-
408 mercaptoethanol, and 0.4 U µl-1 recombinant RNase inhibitor (Clontech) using a Wheaton Dounce
409 tissue grinder. The homogenized tissue was filtered through a 40-µm cell strainer, mixed with an
410 equal volume of working solution (50% OptiPrep density gradient medium (Sigma-Aldrich), 5
411 mM CaCl2, 3 mM Mg(CH3COO)2, 10 mM Tris HCl pH 7.8, 0.1 mM EDTA pH 8.0, and 1 mM
412 β-mercaptoethanol) and loaded on top of an OptiPrep density gradient (29% OptiPrep solution
413 (29% OptiPrep density gradient medium,134 mM sucrose, 5 mM CaCl2, 3 mM Mg(CH3COO)2,
414 10 mM Tris HCl pH 7.8, 0.1 mM EDTA pH 8.0, 1 mM β-mercaptoethanol, 0.04% IGEPAL CA-
415 630, and 0.17 U µl-1 recombinant RNase inhibitor) on top of 35% OptiPrep solution (35%
416 OptiPrep density gradient medium, 96 mM sucrose, 5 mM CaCl2, 3 mM Mg(CH3COO)2, 10 mM
417 Tris HCl pH 7.8, 0.1 mM EDTA pH 8.0, 1 mM β-mercaptoethanol, 0.03% IGEPAL CA-630, and
418 0.12 U µl-1 recombinant RNase inhibitor). The nuclei were separated by ultracentrifugation using
419 an SW32 rotor (5 min, 10,000xG, 4°C). Nuclei were collected from the 29%/35% interphase,
420 washed with PBS containing 0.04% BSA, centrifuged at 300g for 3 min (4 °C), and washed with
421 1 ml of PBS containing 1% BSA. The nuclei were counted and diluted to a concentration of 1,000
422 nuclei per microliter in PBS containing 1% BSA. Libraries were prepared using the Chromium
423 Single Cell 3′ Reagent Kits v.3.1 (Dual Index) according to the manufacturer's protocol (10X
424 Genomics, Pleasanton, CA). The snRNA-seq libraries were sequenced using NextSeq 500/550
425 High Output (150 cycles).
426 **Single nuclei RNA-seq data analysis**
427 Data preprocessing, differential expression, gene ontology analyses
428 Gene counts were retrieved by mapping raw reads to the mouse genome (mm10) using CellRanger
429 software (v 7.0.1). Initial preprocessing of the samples (e.g., removal of ambient noise,
430 identification and removal of contamination from adjacent brain regions, and stressed or damaged
431 cell and low quality cells) were performed using ACTIONet [71]. Downstream analysis was
432 performed in Seurat (v 4.3.0). Nuclei with a minimum 500 unique molecular identifiers (UMIs)
433 and less than 5% mitochondrial genes were considered for downstream analysis. Doublets were
434 identified and removed using scds (v 1.10.0) and genes with no expression was discarded. Count
435 data were log-normalized using NormalizeData and top 2000 highly variable genes were
436 determined using FindVariableFeatures. Expression of these genes were subsequently used to
437 scale gene expression to zero mean and unit variance with ScaleData function. Scaled data was
438 further regressed out for mitochondrial percentage. Top 75 principal components were estimated
439 using RunPCA and aligned with Harmony to account for technical batch effects considering
440 individual sample as batch. Optimum number of principle components (PCs) were determined

441 based on the ElbowPlot and the first 16 PCs was used as input for downstream analyses. A
442 neighborhood graph was constructed based on the Euclidean distance metric in the adjusted PC
443 space using FindNeighbors, and nuclei were clustered using the Louvain method in FindClusters
444 at resolution 0.2. RunUMAP functions with min.dist = 0.5 and spread = 0.5 were used to calculate
445 two-dimensional UMAP coordinates and nuclei clusters were visualized using DimPlot. Cell type
446 specific clusters were annotated using canonical markers. Nuclei clusters expressing mixed cell
447 type specific markers were discarded. Cell type specific marker genes were identified based on the
448 differential expression of each cell type against all other cell types using FindMarkers and genes
449 with significance (adjusted P value<0.05) and increased expression were only considered for cell
450 type specific markers. Differential gene expression analysis was performed using MAST (v
451 1.20.0). Genes with log2 fold change >0.1 and adjusted p value <0.05 were defined as differentially
452 expressed. Module score was calculated using AddModuleScore in Seurat. Gene ontology analyses
453 were performed using either Gene ontology (http://geneontology.org) or Metascape
454 (https://www.metascape.org/). For supervised GO module analysis particularly for oxidative
455 phosphorylation (GO:0006119) and cellular respiration (GO:0045333), we retrieved genes related
456 to these GO terms using gconvert function of gprofiler2 (v 0.2.1). Co-expression GO module
457 score was calculated using AddModuleScore function in Seurat.
458
459 Weighted gene co-expression analysis
460 Weighted gene co-expression analysis (WGCNA) was performed as previously described in
461 [31,72,73]. Briefly, "metacells" were constructed computing mean expression from 25 neighbors
462 using k-nearest neighbors. Normalized and scaled metacells were then used to calculate pair-wise
463 correlations between all gene pairs. Subsequently, based on the approximate scale-free topology,
464 a threshold power of 4 was selected to emphasize the stronger correlations and to compute pair-
465 wise topological overlap to construct a signed network. Modules with minimum size of 25 and
466 deep split of 4 were used for the analysis. Closely related modules were merged using dissimilarity
467 correlation threshold of 0.2. Modules were summarized as network of modular eigengenes (MEs),
468 which was defined based on the first major component of the module and used to compare between
469 the two groups. Module membership of genes was defined as the correlation of gene expression
470 profile with MEs. Hub genes were defined based on the intra-modular connectivity (kME) and top
471 25 hub genes were plotted using igraph package (v 1.3.1). Association between hub module genes
472 and transcription factors was analyzed using ChEA3 [74].
473
474
475 Analyses of granule cells
476 To select granule cells (GCs) we first filtered the snRNA-seq data based on the expression level
477 of Prox1, which is a pan GC marker. Only cells with an expression level of Prox1 greater than 1
478 were retained for subsequent analyses. Cells were normalized, scaled, harmonized and top 30
479 components were used to construct cell clusters and UMAP at resolution of 0.8. Cluster specific
480 marker genes were defined using FindAllMarkers (only.pos = TRUE, min.pct = 0.25, assay =

481 “RNA”) and top 200 genes were used to perform gene enrichment analyses with granule cell
482 specific markers defined in the previous study [75]. Based on the enrichment results, cell clusters
483 were annotated into glial (radial glial), and granule cells (neuroblasts, mature and immature).
484 Clusters that did not show overlap to the marker genes were labeled as unknown cluster type.
485 Annotated granule cells (immature, mature, neuroblasts) were considered for downstream analyses
486 and pseudotime analysis was performed using Monocle. Briefly, we kept the original clustering
487 and dimension reduction from Seurat and created a Monocle cell data set (CDS) using the
488 new_cell_data_set function and treated all cells as a single partition. For trajectory analysis,
489 learn_graph function was used to learn the trajectory graph of the cells. Cells were subsequently
490 assigned a pseudotime value based on their projection on the principal graph learned in
491 the learn_graph function and order_cells function was used to order cells along the trajectory. To
492 find genes whose expression changes along the pseudotime, we then applied a generalized additive
493 model along the principal trajectory via graph_test function. Genes with q-value less than 0.05
494 were considered only for downstream analysis. Top 100 pseudotime associated genes were
495 visualized as heatmap using Heatmap function. Genes that are differentially expressed between
496 ambient and stimulation groups along the trajectory were determined using fit_models with q-
497 value cutoff set at 0.05. Gene ontology analysis was performed using Metascape and
498 ClusterProfiler.
499
500 Analyses of published datasets
501 Hippocampal bulk RNA-seq raw data pertaining to 4, 8, 12 and 18 months of wild type mice were
502 retrieved from GSE168137 and analyzed. Single cell RNA-seq data from frontal cortex and
503 striatum of 4 weeks and 90 weeks of mice was retrieved from GSE207848 and processed in house.
504 List of downregulated genes in excitatory neurons of old individuals compared to young subjects
505 were retrieved from [76]. Cortical and hippocampal bulk RNA-seq data related to Ts65Dn and
506 littermate controls were downloaded from GSE213500 and processed in house. List of
507 downregulated genes in the excitatory neurons of prefrontal cortex from patients with Down
508 syndrome was retrieved from the provided supplementary file in [77]. Bulk RNA-seq data related
509 to 5xFAD and wild type mice of 4 and 8 months were downloaded from GSE168137 and analyzed
510 in house. Single cell data related to 5xFAD and wild type mice of 7 months old were retrieved
511 from GSE140511 and processed in house. Hippocampal excitatory neuronal transcriptomic data
512 from individuals with Alzheimer´s disease and controls were provided by [52]. For Bulk RNA-seq
513 data, genes with low no expression were removed. Differential expression analysis was performed
514 using DESeq2 (v 1.34.0). Genes with FDR<0.05 were defined as differentially expressed. For
515 single cell data related to aging and AD, data were processed as described above using Seurat and
516 cell clusters were visualized in UMAP space. Cell clusters enriched for Slc17a7/VGLUT1, marker
517 for excitatory neuron, were further analyzed for differential expression analysis. Differentially
518 expressed genes (FDR <0.05, abs(log2FC)>0.1) in the SLC7A7+ human hippocampal snRNA-seq
519 data were determined after adjusting for age, sex, and post-mortem interval. Differential
520 expression analyses were performed using MAST. Module score in bulk RNA-seq data was

521 computed using svd as implemented in moduleEigengene of WGCNA package. Hypergeometric
522 overlap analysis was performed using GeneOverlap package in R.
523
524
525 **Immunohistochemistry**
526 24 hours after the final stimulation session, mice were transcardially perfused with 40 ml of ice-
527 cold phosphate buffered saline (PBS) followed by 40 ml of 4% paraformaldehyde (PFA) in PBS.
528 Brains were removed and post-fixed in 4% PFA overnight at 4°C and transferred to PBS prior to
529 sectioning. Brains were sectioned 40 µm thick with a Leica VT1000S vibratome (Leica). Sections
530 were permeabilized and blocked in PBS with 0.3% Triton X-100 and 10% donkey serum at room
531 temperature for 2-hrs. Sections were incubated overnight at 4°C in primary antibody containing
532 PBS with 0.3% Triton X-100 and 10% donkey serum. Primary antibodies were anti-synaptophysin
533 (Synaptic Systems, 101004), anti-PSD95 (Abcam, ab18258), anti-Ki67 (Abcam, ab15580), anti-
534 cFos (Santa Cruz Biotech, sc-166940), anti-Reelin (Millipore Sigma, MAB5364), anti-TCF4
535 (Protein Tech, 13838-1-AP), anti-NeuN (Synaptic Systems, 266004). The following day, brain
536 sections were incubated with fluorescently conjugated secondary antibodies (Jackson
537 ImmunoResearch) for 2 hours at room temperature, and nuclei were stained with DAPI
538 (Invitrogen, D1306). Images were acquired using a confocal microscope (LSM 710; Zeiss or LSM
539 900; Zeiss).
540
541 EdU Staining
542 EdU staining was conducted using the Click-iT™ EdU imaging kit (ThermoFisher, C10340)
543 according to the manufacturer's protocol. This protocol is normally intended for use in cell culture
544 but was adapted for histological staining of brain tissue. Each mouse was intraperitoneally injected
545 with EdU 25 mg/kg for 2 days prior to perfusion. Slides containing mounted frozen brain sections
546 were allowed to thaw to room temperature and then fixed with 4% paraformaldehyde in phosphate
547 buffer saline (PBS) for 15 min. After washing twice with 3% bovine serum albumin (BSA) in PBS,
548 the sections were permeablized with 0.5% Triton X-100 in PBS for 20 min. The sections were
549 again washed twice with 3% BSA in PBS and then incubated with a Click-iT™ reaction cocktail
550 containing Click-iT™ reaction buffer, $CuSO_4$, Alexa Fluor® 594 Azide, and reaction buffer
551 additive for 30 min while protected from light. The sections were washed once more with 3% BSA
552 in PBS before being mounted and imaged.
553
554 **Image analysis**
555 c-Fos quantification
556 Images acquired at 20x magnification and whole hippocampal cFos+ nuclei were analyzed in
557 Imaris (v 10.2). Briefly, surfaces were generated for both cFos and DAPI and cFos+ nuclei were
558 quantified by identifying DAPI+ nuclei overlapping with cFos signals. To account for technical
559 bias, the percentage of cFos+ nuclei was calculated relative to the total number of analyzed nuclei.
560

561 Quantification of colocalization of synaptophysin and PSD95
562 Following the image acquisition using 63x objective, files were imported into Imaris (v9.9). First,
563 the Spots feature of the software was utilized to detect PSD95 and synaptophysin puncta. For each
564 fluorescence channel, minimum and maximum intensity values were collected from every image
565 to maximize detection of puncta and minimize background noise. Means calculated from these
566 minimum and maximum intensity values became the intensity thresholds for the Spots applied to
567 every image. The Spots using the cohort's shared threshold values were applied to one sample
568 image, then saved as a Macro and applied to all other images. After applying Spots, the
569 colocalization function was executed to mark and quantify points from each Spots channel that
570 were within 2um of each other. To validate this proxy method for quantifying mature functional
571 synapses, another method for colocalization analysis was also executed. To do this, the Imaris
572 software's Colocalization Channel function was used. Minimum and maximum thresholds were
573 once again collected from each fluorescence channel to build the new colocalization channel. After
574 calculating the means of the threshold values in each, the channel was built and manually added
575 to every image file. Spots were then added to the new channel to register and quantify the
576 colocalized points detected. Data was analyzed from both methods of analysis to confirm trend.
577 To quantify Reln+ neurons, brain slices were immunostained with anti-Reelin, anti-NeuN and
578 DAPI and images were acquired using the 20x objective in LSM 900. Image analysis was
579 performed using Imaris (v9.9 and v10.2). First, we created surfaces for Reln and NeuN
580 individually. Then, we counted the number of Reln surfaces that overlapped with those of NeuN
581 to identify Reln+ neurons. We calculated the ratio of Reln+ neurons to the total number of neurons
582 to determine the proportion of Reln+ neurons.
583
584 To investigate TCF4 expression changes between the two groups, we performed immunostaining
585 experiment using anti-TCF4 and DAPI on brain slices and acquired images (20x, LSM900) from
586 the dentate gyrus, CA1 and CA3 of the hippocampus. For TCF4 mean intensity analysis, we used
587 the Measure function in ImageJ software (v2.14.0/1.54f). To minimize the technical bias, we
588 averaged the TCF4 intensity across all replicates for each mouse and normalized it to the mean
589 DAPI signal for all control samples.
590
591 **Statistical Analyses**
592 Statistical analysis was conducted in R (v 4.1.2) or Prism (v 8). Statistical details of the
593 experiments, including the statistical tests used, exact value of n, definition of measures can be
594 found in the corresponding figure legends. Unless otherwise stated, statistical significance was set
595 at 0.05.
596
597 **Acknowledgements**
598 We are grateful to the following individuals and organizations for their kind contributions and
599 support of this work: the Alana Down syndrome Center at MIT and the Alana USA Foundation,
600 Inc, National Science Foundation Graduate Research Fellowship under Grant No.1122374, "la

Caixa" Banking Foundation and fellowships for DRA, MRI is a EMBO long term postdoctoral fellow, MM was supported with fellowships from Barbara J. Weedon, Henry E. Singleton, the Hubolow family. ESB acknowledges HHMI and Charles Hieken. We are also thankful to Dr Nancy Kopell, Dr Michelle McCarthy and Tsai lab members for their helpful comments during preparation of this manuscript.

Figure Legends

Fig 1. Multisensory gamma stimulation improves spatial working memory in Ts65Dn mice. A) Experimental scheme. B) Novel Object Recognition (NOR) test. Quantification of recognition index during NOR. Average Novel object exploration time: ambient: 9.73 seconds, stimulation: 12.84 seconds. Average familiar object exploration time: ambient: 10.31 seconds, stimulation: 7.20 seconds. C) Novel Object Location (NOL) test. Quantification of recognition index during NOL. Average Novel location exploration time: ambient: 9.33 seconds, stimulation: 14.72 seconds. Average old location exploration time: ambient: 10.70 seconds, stimulation: 5.34 seconds. D) Spontaneous alteration based on Y-maze. Quantification of percent alteration and total number of entries. ambient = 12, stimulation = 12, unpaired t-test, two-tailed, *P<0.05, ****P<0.0001. Error bars indicate mean ± standard error mean.

Fig 2. Molecular signatures underlying multisensory gamma stimulation-associated cognitive benefits in the hippocampus. A) Experimental scheme for the single nuclei RNA-seq experiment in Ts65Dn mice B) Unbiased clustering of hippocampal snRNA-seq data for 15884 nuclei represented on a UMAP. Cell types are annotated based on the marker genes. Ex: Excitatory Neurons, Astro: Astrocytes, Oligo: Oligodendrocytes, In: Inhibitory Neurons, OPC: Oligodendrocyte precursor cells, Micro: Microglia. C) Heatmap showing number of differentially expressed genes in excitatory and inhibitory neurons in the hippocampal snRNA-seq data from stimulation vs ambient Ts65Dn mice. D) Gene ontology analyses for the upregulated and downregulated genes in hippocampal excitatory and inhibitory neurons in stimulation vs ambient Ts65Dn mice. Color represents statistical significance after multiple testing adjustments. E) Signed bar plot displaying significant co-expression changes of the identified 7 gene modules in hippocampal excitatory neurons in stimulation vs ambient TsD65n mice. Red color denotes increased and blue color decreased expression in stimulated mice. X-axis represents signed -log10 p value. F) Hub genes of modules Ex-3, Ex-6 and Ex-7. Genes that encode synaptic proteins are highlighted in green. G) Top gene ontology biological processes for modules Ex-3, Ex-6, and Ex-7. H) Quantification of mature synapses in granule cell molecular layer of dentate gyrus in stimulation and ambient Ts65Dn mice via co-localization of PSD95 and synaptophysin. Representative images of mouse brain slices stained with PSD95, synaptophysin and DAPI. Images were acquired using 63x objective. Triangles indicate colocalized puncta. Y-axis represents the absolute number of colocalized puncta. Scale bar = 10 microns. t-test, two-tailed, unpaired, *P<0.05. Error bars indicate mean ± sem. ambient = 6, stimulation = 7 mice. I) Hub genes overlapping with disease risk genes for Alzheimer´s disease. J) Quantification of *Reln*+ neurons after ambient or 40Hz stimulation. Representative confocal images of hippocampal CA3

642 area brain slices from Ts65Dn mice after staining for Reelin and NeuN with DAPI counterstain.
643 Merged panel shows all three markers. 20x objective. Scale bar = 50 pixels. Bar plots show the
644 mean proportion of *Reln*+ neurons between the ambient and stimulation groups. Error bars indicate
645 mean ± sem. t-test, two-tailed, unpaired, **P<0.01. Number of mice = 5/group. K-L)
646 Hypergeometric overlap of the genes in modules Ex-3, Ex-6, and Ex-7 with different sets of
647 downregulated genes related to (K) aging and (L) Alzheimer's disease (AD). Color represents fold
648 enrichment. *FDR<0.05, **FDR<0.01, ***FDR<0.001.
649
650 **Fig 3. Multisensory gamma stimulation increases adult neurogenesis in Ts65Dn mice.**
651 A) Top 10 ranked TFs for module Ex-7. Color represents -log10 enrichment score based on ChEA3
652 analysis. B) Mean TCF4 fluorescence intensity after treatment of mice with or without 40 Hz
653 stimulation. Representative images of TS65Dn mouse brain slices from the hippocampal granule
654 cell molecular layer of dentate gyrus area after staining for TCF4 (green) and DAPI (blue). Merged
655 panel shows both markers. Scale bar = 15 µm. Bar plots show normalized mean intensity (% of
656 ambient group) between the two groups. t-test, two-tailed, unpaired. *P<0.05. number of mice =
657 4/group. C) Sub clusters of immature granule cells represented on a UMAP D) Dot plots showing
658 relative enrichment of marker genes across the three sub-clusters of immature granule cells (GC)
659 E) UMAP plots separated by group reveal differential numbers of cluster 3 immature GC in
660 stimulation group. F) Box plot shows increased proportion of Prox1+ immature GC cells in
661 stimulation vs ambient Ts65Dn mice. Center line represents the median; lower and the upper lines
662 represent the 25th and 75th percentiles, respectively; whiskers indicate the smallest and largest
663 values in the 1.5x interquartile range. G-H) Increased cell proliferation in the dentate gyrus of
664 stimulation vs ambient Ts65Dn mice tested via immunolabeling for G) Ki67 (ambient = 6 mice,
665 stimulation = 4 mice); Scale bar = 10 µm. and H) EdU (ambient = 8 mice, stimulation = 8 mice);
666 Scale bar = 50 microns. Error bar indicates mean ± standard error mean. Two tailed, unpaired t-
667 test. *P<0.05, **P<0.01, ***P<0.001.
668
669 ## Supplementary Figures
670 **Fig S1. Multisensory gamma stimulation does not affect locomotor and anxiety-like behavior**
671 **in Ts65Dn mice.** A) Quantification of total distance traveled during open field test B)
672 Quantification of time spent in the center. Error bars indicate mean ± standard deviation, unpaired
673 t-test, two-tailed, ambient = 12, stimulation = 12.
674
675 **Fig S2. Multisensory gamma stimulation increases c-Fos positive nuclei in the hippocampus**
676 **of Ts65Dn mice.** A) Experimental outline. B) Representative images of c-Fos+ nuclei in the
677 hippocampus after ambient or 40 Hz stimulation. Blue represents DAPI and green represents c-
678 Fos signals. Scale bar = 200 µm. C) Bar plots showing the percentage of c-Fos+ nuclei in the two
679 groups. N = 4 mice /group. Error bar indicates mean ± sem. Two-tailed, unpaired t-test, *P<0.05.
680

681 **Fig S3. Quality control of the hippocampal snRNA-seq data from Ts65Dn mice.** Distribution
682 of A) number of genes B) number of UMI, C) complexity and D) mitochondrial percentage across
683 15884 nuclei (ambient: 7665, stimulation: 8219). E) Canonical cell type specific marker
684 expression in cognate cell types. Slc17a7, Camk2a in excitatory neurons; Gad1, Gad2 in inhibitory
685 neurons; Pdgfra, Vcan in OPC; Mbp, Plp1 in Oligodendrocytes; Slc1a3, Aqp4 in Astrocytes;
686 Csf1r, Hexb in microglia; Pdgfrb, Cldn5 in vascular cells, KI, Slc26a11, Cldn1 in choroid plexus
687 cells. F) Pie chart displaying the distribution of detected cell types. G) Nuclei from stimulation and
688 ambient Ts65Dn mice groups are well integrated. H) Proportion of nuclei detected across cell types
689 in both groups. I) Volcano plots showing genes that are significantly altered in excitatory and
690 inhibitory neurons in the stimulation group compared to the ambient group.
691
692 **Fig S4. Top biological processes downregulated in Ts65Dn mice and individuals with DS.** A)
693 Differential gene expression observed in bulk RNA-seq data from hippocampi and cortices of
694 Ts65Dn mice (n = 6) and littermate controls (n = 6). Data were retrieved from GSE213500. Gene
695 counts were normalized and differential expression analysis was performed using DESeq2 after
696 adjusting for region specific difference. B) Gene ontology analyses revealed that the genes related
697 to mRNA processing, synapse organization and cognition are downregulated in Ts65Dn mice
698 compared to the controls. C) GO analysis of genes downregulated in excitatory neurons of *post*
699 *mortem* brains of individuals with DS compared to healthy subjects. Gene expression changes data
700 were retrieved from Palmer CR et al[61].
701
702 **Fig S5. Weighted gene co-expression analysis.** A) Cluster dendrogram for seven excitatory gene
703 modules. B) soft-power threshold was determined based on scale-free topology measure and mean
704 connectivity (see Methods). C) Hub genes of Ex-1 and Ex-2 module.
705
706 **Fig S6. Immunostaining-based analysis of putative synapses in the hippocampal CA1 region**
707 **between ambient and stimulation groups.** (Left) Representative images showing PSD95 and
708 Synaptophysin co-localization. White arrows indicate colocalized puncta. Scale bar = 10 µm.
709 (Right) Bar plots showing the absolute number of colocalized puncta. Statistical significance was
710 determined using a two-tailed, unpaired *t*-test, *N* = 6–7 per group. Error bar: mean ± standard error
711 mean.
712
713 **Fig S7. Immunostaining based analyses of Reln+ neurons in hippocampal DG and CA1**
714 **regions between ambient and stimulation groups.** A) (Left) Representative images of Reln+
715 neurons in the DG granule cell layer of the hippocampus. (Right) Barplots show percentages of
716 Reln+ neuorns between two groups. 40 Hz stimulation increased percentages of Reln+ neurons in
717 DG of DS mice. Scale bar = 20 µm. Two-tailed t-test, **P<0.01, N = 5 per group. B) (Left)
718 Representative images of Reln+ neurons in the hippocampal CA1 region. (Right) Barplots show
719 percentages of Reln+ neuorns between two groups. Scale bar = 10 µm. Two-tailed, unpaired t-test,
720 N = 5 per group.

721
722
723 **Fig S8. Co-expression pattern of excitatory gene modules along aging.** Expression patterns of
724 module Ex-3, Ex-6 and Ex-7 display reduced co-expression at old age (18 months). Boxplots show
725 changes in gene module expression along aging in the hippocampus. Y-axis shows gene module
726 expression eigenvalue. In the box plots, median is marked with the center line, while the lower and
727 the upper lines represent the 25th and 75th percentiles, respectively. The whiskers indicate the
728 smallest and largest values respectively in the 1.5x interquartile range. P-value determined by
729 Kruskal-Wallis test.
730
731 **Fig S9. TCF4 expression in the hippocampal CA1 and CA3 between ambient and stimulation**
732 **groups**. A) (Left) Representative images of TCF4 expression in the CA1 region of the
733 hippocampus. (Right) Bar plots showing normalized mean intensity (% of the ambient group)
734 between the two groups. Two-tailed, unpaired *t*-test, N = 4 per group. Scale bar = 30 µm. B) (Left)
735 Representative images of TCF4 expression in the CA3 region of the hippocampus. (Right) Bar
736 plots showing normalized mean intensity (% of the ambient group) between the two groups. Two-
737 tailed *t*-test, N = 4 per group. Scale bar = 30 µm.
738
739 **Fig S10: Identification of hippocampal immature GCs.** A) Prox1+ hippocampal nuclei were
740 sorted *in silico*, clustered, and visualized on a UMAP. Cell clusters were annotated based on
741 marker genes. Neuroblasts and GCs were selected for downstream analyses. B) Pseudotime
742 analysis was performed to gain better insights into granule cell maturation. Cells are color coded
743 based on the inferred progression along the maturation trajectory. The color code represents the
744 relative pseudotime values, with yellow indicating cells at the earlier stage of maturation and dark
745 blue indicating cells at the mature stage. C) Immature GC-specific markers were used to further
746 confirm the presence of immature GCs.
747
748 **Fig S11. Multisensory gamma stimulation increases oxidative phosphorylation in a subset of**
749 **immature granule cells.** A) Heatmap showing relative expression of top 100 genes that
750 significantly changed ($q<0.05$) along the maturation trajectory of granule cells (GC) in stimulation
751 vs ambient Ts65Dn mice B) Biological processes representing differentially expressed genes (up
752 and down-regulated) along the maturation trajectory of GC between the stimulation and ambient
753 groups. C) Biological processes for genes differentially expressed between cluster 1,3 and cluster
754 2,3.
755
756
757
758
759
760

Supporting Information

Table S1A-B: List of differentially expressed genes in excitatory and inhibitory neurons after stimulation.

Table S2: Gene enrichment analysis between upregulated genes in excitatory neurons and synaptic genes.

Table S3A-B: List of downregulated genes in Down Syndrome.

Table S4: List of co-expressed module genes identified based on weighted co-expression analysis.

Table S5A-C: List of downregulated genes in aging.

Table S6A-D: List of downregulated genes in Alzheimer's Disease.

Table S7: Top 10 transcription factors associated with module Ex-7.

Table S8: List of differentially expressed following 40Hz stimulation along the granule cell developmental trajectory.

References

1. Guidi S, Bonasoni P, Ceccarelli C, Santini D, Gualtieri F, Ciani E, et al. Neurogenesis impairment and increased cell death reduce total neuron number in the hippocampal region of fetuses with Down syndrome: Hippocampal hypocellularity in down fetuses. Brain Pathol. 2008;18: 180–197.
2. Hanson JE, Blank M, Valenzuela RA, Garner CC, Madison DV. The functional nature of synaptic circuitry is altered in area CA3 of the hippocampus in a mouse model of Down's syndrome: Functional connectivity in Down's syndrome. J Physiol. 2007;579: 53–67.
3. Pennington BF, Moon J, Edgin J, Stedron J, Nadel L. The neuropsychology of Down syndrome: evidence for hippocampal dysfunction. Child Dev. 2003;74: 75–93.
4. Tungate AS, Conners FA. Executive function in Down syndrome: A meta-analysis. Res Dev Disabil. 2021;108: 103802.
5. Hithersay R, Startin CM, Hamburg S, Mok KY, Hardy J, Fisher EMC, et al. Association of dementia with mortality among adults with Down syndrome older than 35 years. JAMA Neurol. 2019;76: 152–160.
6. Martorell AJ, Paulson AL, Suk H-J, Abdurrob F, Drummond GT, Guan W, et al. Multi-sensory gamma stimulation ameliorates Alzheimer's-associated pathology and improves cognition. Cell. 2019;177: 256–271.e22.
7. Adaikkan C, Middleton SJ, Marco A, Pao P-C, Mathys H, Kim DN-W, et al. Gamma entrainment binds higher-order brain regions and offers neuroprotection. Neuron. 2019;102: 929–943.e8.
8. Chan D, Suk H-J, Jackson BL, Milman NP, Stark D, Klerman EB, et al. Gamma frequency sensory stimulation in mild probable Alzheimer's dementia patients: Results of feasibility and pilot studies. PLoS One. 2022;17: e0278412.
9. Murdock MH, Yang C-Y, Sun N, Pao P-C, Blanco-Duque C, Kahn MC, et al. Multisensory gamma stimulation promotes glymphatic clearance of amyloid. Nature. 2024;627: 149–156.
10. Iaccarino HF, Singer AC, Martorell AJ, Rudenko A, Gao F, Gillingham TZ, et al. Gamma frequency entrainment attenuates amyloid load and modifies microglia. Nature. 2016;540: 230–235.
11. He Q, Colon-Motas KM, Pybus AF, Piendel L, Seppa JK, Walker ML, et al. A feasibility trial of gamma sensory flicker for patients with prodromal Alzheimer's disease. Alzheimers Dement (N Y). 2021;7: e12178.
12. Liu C, Han T, Xu Z, Liu J, Zhang M, Du J, et al. Modulating gamma oscillations promotes brain connectivity to improve cognitive impairment. Cereb Cortex. 2022;32: 2644–2656.
13. Cimenser A, Hempel E, Travers T, Strozewski N, Martin K, Malchano Z, et al. Sensory-evoked 40-Hz gamma oscillation improves sleep and Daily Living activities in Alzheimer's disease patients. Front Syst Neurosci. 2021;15: 746859.
14. Guerra A, Asci F, D'Onofrio V, Sveva V, Bologna M, Fabbrini G, et al. Enhancing gamma oscillations restores primary motor cortex plasticity in Parkinson's disease. J Neurosci. 2020;40: 4788–4796.
15. Reeves RH, Irving NG, Moran TH, Wohn A, Kitt C, Sisodia SS, et al. A mouse model for Down syndrome exhibits learning and behaviour deficits. Nat Genet. 1995;11: 177–184.
16. Belichenko PV, Masliah E, Kleschevnikov AM, Villar AJ, Epstein CJ, Salehi A, et al. Synaptic structural abnormalities in the Ts65Dn mouse model of Down Syndrome. J Comp Neurol. 2004;480: 281–298.
17. Clark S, Schwalbe J, Stasko MR, Yarowsky PJ, Costa ACS. Fluoxetine rescues deficient neurogenesis in hippocampus of the Ts65Dn mouse model for Down syndrome. Exp Neurol. 2006;200: 256–261.
18. Kleschevnikov AM, Belichenko PV, Faizi M, Jacobs LF, Htun K, Shamloo M, et al. Deficits in cognition and synaptic plasticity in a mouse model of Down syndrome ameliorated by GABAB receptor antagonists. J Neurosci. 2012;32: 9217–9227.
19. Faizi M, Bader PL, Tun C, Encarnacion A, Kleschevnikov A, Belichenko P, et al. Comprehensive behavioral phenotyping of Ts65Dn mouse model of Down syndrome: activation of β1-adrenergic receptor by xamoterol as a potential cognitive

enhancer. Neurobiol Dis. 2011;43: 397–413.
20. Chung L. A brief introduction to the transduction of neural activity into Fos signal. Balsaenggwa Saengsig. 2015;19: 61–67.
21. Koopmans F, van Nierop P, Andres-Alonso M, Byrnes A, Cijsouw T, Coba MP, et al. SynGO: An evidence-based, expert-curated knowledge base for the synapse. Neuron. 2019;103: 217–234.e4.
22. Cingolani LA, Goda Y. Actin in action: the interplay between the actin cytoskeleton and synaptic efficacy. Nat Rev Neurosci. 2008;9: 344–356.
23. Mei L, Xiong W-C. Neuregulin 1 in neural development, synaptic plasticity and schizophrenia. Nat Rev Neurosci. 2008;9: 437–452.
24. Yasuda R, Hayashi Y, Hell JW. CaMKII: a central molecular organizer of synaptic plasticity, learning and memory. Nat Rev Neurosci. 2022;23: 666–682.
25. Cheadle L, Biederer T. The novel synaptogenic protein Farp1 links postsynaptic cytoskeletal dynamics and transsynaptic organization. J Cell Biol. 2012;199: 985–1001.
26. Lee J-R. Protein tyrosine phosphatase PTPRT as a regulator of synaptic formation and neuronal development. BMB Rep. 2015;48: 249–255.
27. Choi Y, Park H, Jung H, Kweon H, Kim S, Lee SY, et al. NGL-1/LRRC4C deletion moderately suppresses hippocampal excitatory synapse development and function in an input-independent manner. Front Mol Neurosci. 2019;12: 119.
28. Akaneya Y, Sohya K, Kitamura A, Kimura F, Washburn C, Zhou R, et al. Ephrin-A5 and EphA5 interaction induces synaptogenesis during early hippocampal development. PLoS One. 2010;5: e12486.
29. Swarup V, Hinz FI, Rexach JE, Noguchi K-I, Toyoshiba H, Oda A, et al. Identification of evolutionarily conserved gene networks mediating neurodegenerative dementia. Nat Med. 2019;25: 152–164.
30. Rexach JE, Cheng Y, Chen L, Polioudakis D, Lin L-C, Mitri V, et al. Cross-disorder and disease-specific pathways in dementia revealed by single-cell genomics. Cell. 2024;187: 5753–5774.e28.
31. Morabito S, Miyoshi E, Michael N, Shahin S, Martini AC, Head E, et al. Single-nucleus chromatin accessibility and transcriptomic characterization of Alzheimer's disease. Nat Genet. 2021;53: 1143–1155.
32. Gandal MJ, Haney JR, Wamsley B, Yap CX, Parhami S, Emani PS, et al. Broad transcriptomic dysregulation occurs across the cerebral cortex in ASD. Nature. 2022;611: 532–539.
33. Herring A, Donath A, Steiner KM, Widera MP, Hamzehian S, Kanakis D, et al. Reelin depletion is an early phenomenon of Alzheimer's pathology. J Alzheimers Dis. 2012;30: 963–979.
34. Kocherhans S, Madhusudan A, Doehner J, Breu KS, Nitsch RM, Fritschy J-M, et al. Reduced Reelin expression accelerates amyloid-beta plaque formation and tau pathology in transgenic Alzheimer's disease mice. J Neurosci. 2010;30: 9228–9240.
35. Marckx AT, Fritschle KE, Calvier L, Herz J. Reelin changes hippocampal learning in aging and Alzheimer's disease. Behav Brain Res. 2021;414: 113482.
36. Lopera F, Marino C, Chandrahas AS, O'Hare M, Villalba-Moreno ND, Aguillon D, et al. Resilience to autosomal dominant Alzheimer's disease in a Reelin-COLBOS heterozygous man. Nat Med. 2023;29: 1243–1252.
37. Papes F, Camargo AP, de Souza JS, Carvalho VMA, Szeto RA, LaMontagne E, et al. Transcription Factor 4 loss-of-function is associated with deficits in progenitor proliferation and cortical neuron content. Nat Commun. 2022;13: 2387.
38. Chen H-Y, Bohlen JF, Maher BJ. Molecular and cellular function of transcription factor 4 in Pitt-Hopkins syndrome. Dev Neurosci. 2021;43: 159–167.
39. Crux S, Herms J, Dorostkar MM. Tcf4 regulates dendritic spine density and morphology in the adult brain. PLoS One. 2018;13: e0199359.
40. Shariq M, Sahasrabuddhe V, Krishna S, Radha S, Nruthyathi, Bellampalli R, et al. Adult neural stem cells have latent inflammatory potential that is kept suppressed by Tcf4 to facilitate adult neurogenesis. Sci Adv. 2021;7: eabf5606.
41. Braun K, Häberle BM, Wittmann M-T, Lie DC. Enriched environment ameliorates adult hippocampal neurogenesis deficits in Tcf4 haploinsufficient mice. BMC Neurosci. 2020;21: 50.
42. Habib N, Li Y, Heidenreich M, Swiech L, Avraham-Davidi I, Trombetta JJ, et al. Div-Seq: Single-nucleus RNA-Seq reveals dynamics of rare adult newborn neurons. Science. 2016;353: 925–928.
43. Zhou Y, Su Y, Li S, Kennedy BC, Zhang DY, Bond AM, et al. Molecular landscapes of human hippocampal immature neurons across lifespan. Nature. 2022;607: 527–533.
44. Cembrowski MS, Wang L, Sugino K, Shields BC, Spruston N. Hipposeq: a comprehensive RNA-seq database of gene expression in hippocampal principal neurons. Elife. 2016;5: e14997.
45. Choi JHK, Berger JD, Mazzella MJ, Morales-Corraliza J, Cataldo AM, Nixon RA, et al. Age-dependent dysregulation of brain amyloid precursor protein in the Ts65Dn Down syndrome mouse model. J Neurochem. 2009;110: 1818–1827.
46. Holtzman DM, Santucci D, Kilbridge J, Chua-Couzens J, Fontana DJ, Daniels SE, et al. Developmental abnormalities and age-related neurodegeneration in a mouse model of Down syndrome. Proc Natl Acad Sci U S A. 1996;93: 13333–13338.
47. Tallino S, Winslow W, Bartholomew SK, Velazquez R. Temporal and brain region-specific elevations of soluble Amyloid-β40-42 in the Ts65Dn mouse model of Down syndrome and Alzheimer's disease. Aging Cell. 2022;21: e13590.
48. Hunter CL, Bimonte HA, Granholm ACE. Behavioral comparison of 4 and 6 month-old Ts65Dn mice: age-related impairments in working and reference memory. Behav Brain Res. 2003;138: 121–131.
49. Lorenzi HA, Reeves RH. Hippocampal hypocellularity in the Ts65Dn mouse originates early in development. Brain Res. 2006;1104: 153–159.
50. Fortea J, Zaman SH, Hartley S, Rafii MS, Head E, Carmona-Iragui M. Alzheimer's disease associated with Down syndrome: a genetic form of dementia. Lancet Neurol. 2021;20: 930–942.

51. Teller JK, Russo C, DeBusk LM, Angelini G, Zaccheo D, Dagna-Bricarelli F, et al. Presence of soluble amyloid beta-peptide precedes amyloid plaque formation in Down's syndrome. Nat Med. 1996;2: 93–95.
52. Mathys H, Boix CA, Akay LA, Xia Z, Davila-Velderrain J, Ng AP, et al. Single-cell multiregion dissection of Alzheimer's disease. Nature. 2024;632: 858–868.
53. Dupret D, Revest J-M, Koehl M, Ichas F, De Giorgi F, Costet P, et al. Spatial relational memory requires hippocampal adult neurogenesis. PLoS One. 2008;3: e1959.
54. Berdugo-Vega G, Arias-Gil G, López-Fernández A, Artegiani B, Wasielewska JM, Lee C-C, et al. Increasing neurogenesis refines hippocampal activity rejuvenating navigational learning strategies and contextual memory throughout life. Nat Commun. 2020;11: 135.
55. Bianchi P, Ciani E, Guidi S, Trazzi S, Felice D, Grossi G, et al. Early pharmacotherapy restores neurogenesis and cognitive performance in the Ts65Dn mouse model for Down syndrome. J Neurosci. 2010;30: 8769–8779.
56. Goldberg M, Islam MR, Kerimoglu C, Lancelin C, Gisa V, Burkhardt S, et al. Exercise as a model to identify microRNAs linked to human cognition: a role for microRNA-409 and microRNA-501. Transl Psychiatry. 2021;11: 514.
57. Fischer A, Sananbenesi F, Wang X, Dobbin M, Tsai L-H. Recovery of learning and memory is associated with chromatin remodelling. Nature. 2007;447: 178–182.
58. Contestabile A, Greco B, Ghezzi D, Tucci V, Benfenati F, Gasparini L. Lithium rescues synaptic plasticity and memory in Down syndrome mice. J Clin Invest. 2013;123: 348–361.
59. Fernandez F, Morishita W, Zuniga E, Nguyen J, Blank M, Malenka RC, et al. Pharmacotherapy for cognitive impairment in a mouse model of Down syndrome. Nat Neurosci. 2007;10: 411–413.
60. Parrini M, Ghezzi D, Deidda G, Medrihan L, Castroflorio E, Alberti M, et al. Aerobic exercise and a BDNF-mimetic therapy rescue learning and memory in a mouse model of Down syndrome. Sci Rep. 2017;7: 16825.
61. Zhou W-B, Miao Z-N, Zhang B, Long W, Zheng F-X, Kong J, et al. Luteolin induces hippocampal neurogenesis in the Ts65Dn mouse model of Down syndrome. Neural Regen Res. 2019;14: 613–620.
62. Aziz NM, Guedj F, Pennings JLA, Olmos-Serrano JL, Siegel A, Haydar TF, et al. Lifespan analysis of brain development, gene expression and behavioral phenotypes in the Ts1Cje, Ts65Dn and Dp(16)1/Yey mouse models of Down syndrome. Dis Model Mech. 2018;11. doi:10.1242/dmm.031013
63. Herault Y, Delabar JM, Fisher EMC, Tybulewicz VLJ, Yu E, Brault V. Rodent models in Down syndrome research: impact and future opportunities. Dis Model Mech. 2017;10: 1165–1186.
64. Martínez-Cué C, Baamonde C, Lumbreras M, Paz J, Davisson MT, Schmidt C, et al. Differential effects of environmental enrichment on behavior and learning of male and female Ts65Dn mice, a model for Down syndrome. Behav Brain Res. 2002;134: 185–200.
65. Sago H, Carlson EJ, Smith DJ, Rubin EM, Crnic LS, Huang TT, et al. Genetic dissection of region associated with behavioral abnormalities in mouse models for Down syndrome. Pediatr Res. 2000;48: 606–613.
66. Shaw PR, Klein JA, Aziz NM, Haydar TF. Longitudinal neuroanatomical and behavioral analyses show phenotypic drift and variability in the Ts65Dn mouse model of Down syndrome. Dis Model Mech. 2020;13: dmm046243.
67. Suk H-J, Buie N, Xu G, Banerjee A, Boyden ES, Tsai L-H. Vibrotactile stimulation at gamma frequency mitigates pathology related to neurodegeneration and improves motor function. Front Aging Neurosci. 2023;15: 1129510.
68. Singer AC, Martorell AJ, Douglas JM, Abdurrob F, Attokaren MK, Tipton J, et al. Noninvasive 40-Hz light flicker to recruit microglia and reduce amyloid beta load. Nat Protoc. 2018;13: 1850–1868.
69. Leger M, Quiedeville A, Bouet V, Haelewyn B, Boulouard M, Schumann-Bard P, et al. Object recognition test in mice. Nat Protoc. 2013;8: 2531–2537.
70. Mathys H, Davila-Velderrain J, Peng Z, Gao F, Mohammadi S, Young JZ, et al. Single-cell transcriptomic analysis of Alzheimer's disease. Nature. 2019;570: 332–337.
71. Mohammadi S, Davila-Velderrain J, Kellis M. A multiresolution framework to characterize single-cell state landscapes. Nat Commun. 2020;11: 5399.
72. Islam MR, Kaurani L, Berulava T, Heilbronner U, Budde M, Centeno TP, et al. A microRNA signature that correlates with cognition and is a target against cognitive decline. EMBO Mol Med. 2021;13: e13659.
73. Morabito S, Reese F, Rahimzadeh N, Miyoshi E, Swarup V. hdWGCNA identifies co-expression networks in high-dimensional transcriptomics data. Cell Rep Methods. 2023;3: 100498.
74. Keenan AB, Torre D, Lachmann A, Leong AK, Wojciechowicz ML, Utti V, et al. ChEA3: transcription factor enrichment analysis by orthogonal omics integration. Nucleic Acids Res. 2019;47: W212–W224.
75. Hochgerner H, Zeisel A, Lönnerberg P, Linnarsson S. Conserved properties of dentate gyrus neurogenesis across postnatal development revealed by single-cell RNA sequencing. Nat Neurosci. 2018;21: 290–299.
76. Huang K, Gong H, Guan J, Zhang L, Hu C, Zhao W, et al. AgeAnno: a knowledgebase of single-cell annotation of aging in human. Nucleic Acids Res. 2023;51: D805–D815.
77. Palmer CR, Liu CS, Romanow WJ, Lee M-H, Chun J. Altered cell and RNA isoform diversity in aging Down syndrome brains. Proc Natl Acad Sci U S A. 2021;118: e2114326118.

Fig 1

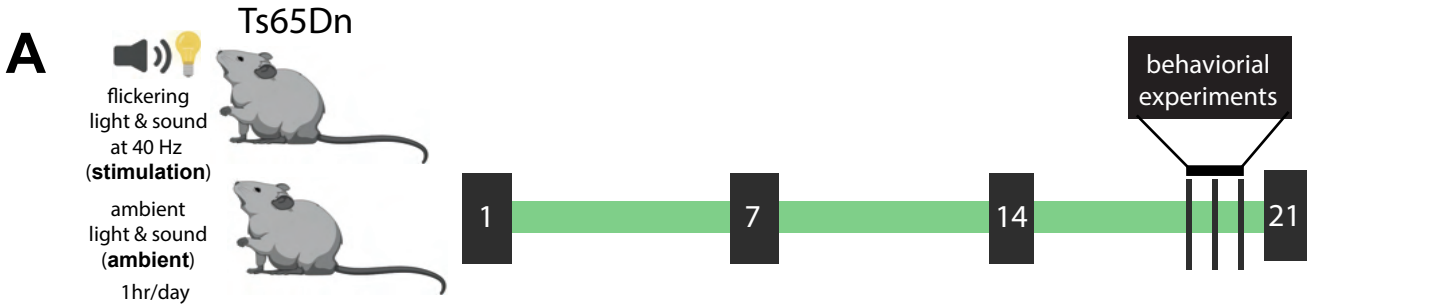
A
Ts65Dn
flickering light & sound at 40 Hz (stimulation)
ambient light & sound (ambient)
1hr/day
1
7
14
21
behaviorial experiments

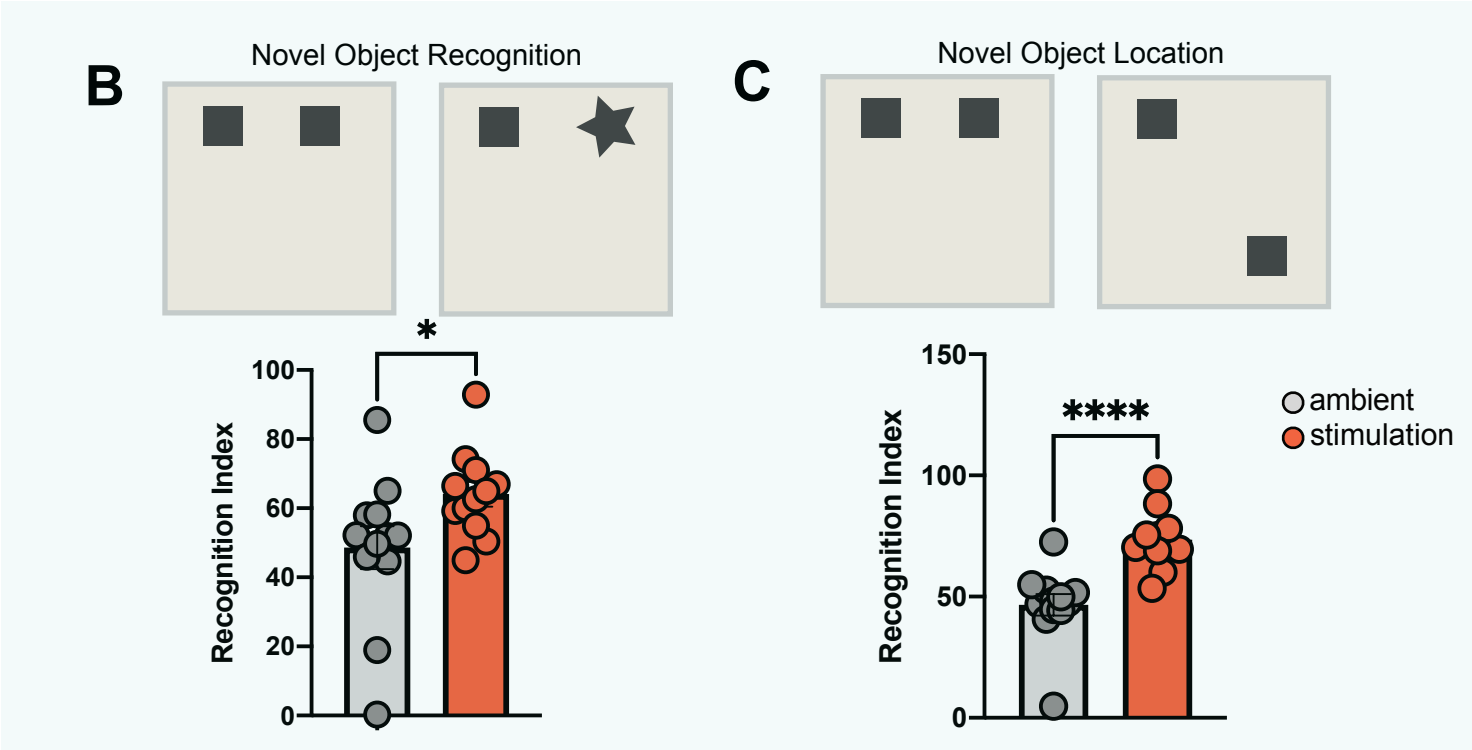
B
Novel Object Recognition
Recognition Index
100
80
60
40
20
0
*
C
Novel Object Location
Recognition Index
150
100
50
0
****
ambient
stimulation

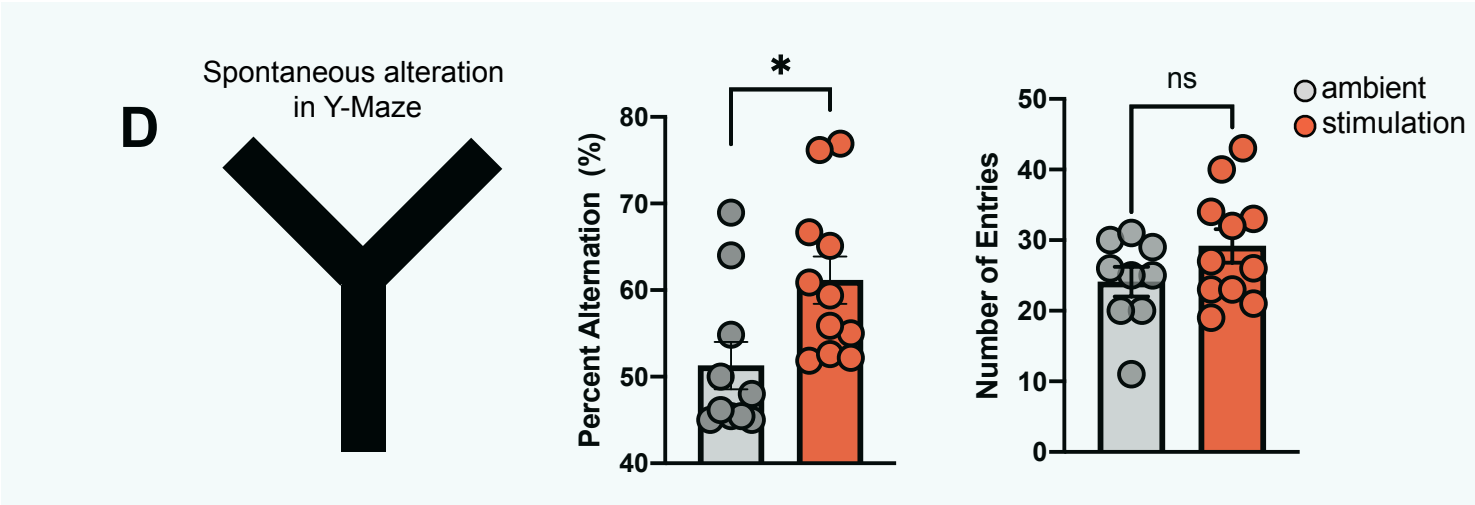
D
Spontaneous alteration in Y-Maze
Percent Alternation (%)
80
70
60
50
40
*
Number of Entries
50
40
30
20
10
0
ns
ambient
stimulation

Fig 2

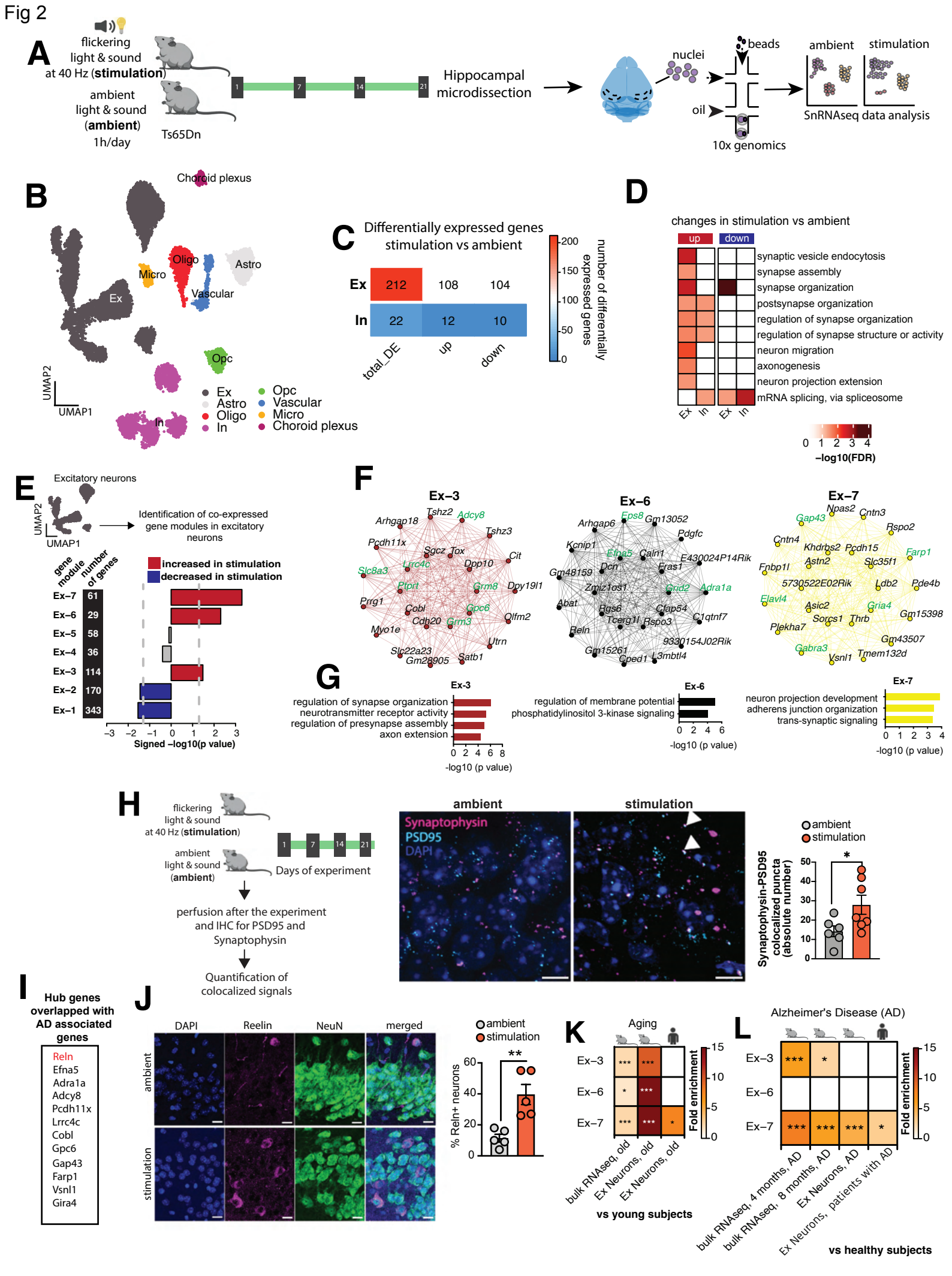
A
flickering light & sound at 40 Hz (stimulation)
ambient light & sound (ambient) 1h/day
Ts65Dn
1
7
14
21
Hippocampal microdissection
nuclei
beads
oil
10x genomics
ambient
stimulation
SnRNAseq data analysis
B
Choroid plexus
Oligo
Astro
Micro
Vascular
Ex
Opc
In
UMAP2
UMAP1
Ex
Astro
Oligo
In
Opc
Vascular
Micro
Choroid plexus
C
Differentially expressed genes stimulation vs ambient
Ex 212 108 104
In 22 12 10
total_DE
up
down
number of differentially expressed genes
200
150
100
50
0
D
changes in stimulation vs ambient
up
down
synaptic vesicle endocytosis
synapse assembly
synapse organization
postsynapse organization
regulation of synapse organization
regulation of synapse structure or activity
neuron migration
axonogenesis
neuron projection extension
mRNA splicing, via spliceosome
Ex
In
Ex
In
0 1 2 3 4
−log10(FDR)
E
Excitatory neurons
UMAP2
UMAP1
Identification of co-expressed gene modules in excitatory neurons
gene module
number of genes
increased in stimulation
decreased in stimulation
Ex−7 61
Ex−6 29
Ex−5 58
Ex−4 36
Ex−3 114
Ex−2 170
Ex−1 343
−3 −2 −1 0 1 2 3
Signed −log10(p value)
F
Ex−3
Tshz2
Adcy8
Arhgap18
Tshz3
Pcdh11x
Sgcz
Tox
Cit
Lrrc4c
Dpp10
Slc8a3
Ptprt
Grm8
Dpy19l1
Prrg1
Cobl
Gpc6
Olfm2
Cdh20
Grm3
Myo1e
Utrn
Slc22a23
Gm28905
Satb1
Ex−6
Eps8
Gm13052
Arhgap6
Pdgfc
Kcnip1
Efna5
Caln1
E430024P14Rik
Dcn
Fras1
Gm48159
Zmiz1os1
Grid2
Adra1a
Abat
Rgs6
Cfap54
Tcerg1l
Rspo3
C1qtnf7
Reln
9330154J02Rik
Gm15261
Cped1
L3mbtl4
Ex−7
Npas2
Gap43
Cntn3
Rspo2
Cntn4
Khdrbs2
Pcdh15
Farp1
Astn2
Slc35f1
Fnbp1l
5730522E02Rik
Ldb2
Pde4b
Elavl4
Asic2
Gria4
Gm15398
Sorcs1
Thrb
Plekha7
Gm43507
Gabra3
Vsnl1
Tmem132d
G
Ex-3
regulation of synapse organization
neurotransmitter receptor activity
regulation of presynapse assembly
axon extension
0 2 4 6 8
-log10 (p value)
Ex-6
regulation of membrane potential
phosphatidylinositol 3-kinase signaling
0 2 4 6
-log10 (p value)
Ex-7
neuron projection development
adherens junction organization
trans-synaptic signaling
0 1 2 3 4
-log10 (p value)
H
flickering light & sound at 40 Hz (stimulation)
ambient light & sound (ambient)
1
7
14
21
Days of experiment
perfusion after the experiment and IHC for PSD95 and Synaptophysin
Quantification of colocalized signals
ambient
stimulation
Synaptophysin
PSD95
DAPI
ambient
stimulation
Synaptophysin-PSD95 colocalized puncta (absolute number)
50
40
30
20
10
0
*
I
Hub genes overlapped with AD associated genes
Reln
Efna5
Adra1a
Adcy8
Pcdh11x
Lrrc4c
Cobl
Gpc6
Gap43
Farp1
Vsnl1
Gira4
J
DAPI
Reelin
NeuN
merged
ambient
stimulation
ambient
stimulation
**
% Reln+ neurons
60
40
20
0
K
Aging
Ex−3
Ex−6
Ex−7
Fold enrichment
15
10
5
0
bulk RNAseq, old
Ex Neurons, old
Ex Neurons, old
vs young subjects
L
Alzheimer's Disease (AD)
Ex−3
Ex−6
Ex−7
Fold enrichment
15
10
5
0
bulk RNAseq, 4 months, AD
bulk RNAseq, 8 months, AD
Ex Neurons, AD
Ex Neurons, patients with AD
vs healthy subjects

Fig 3

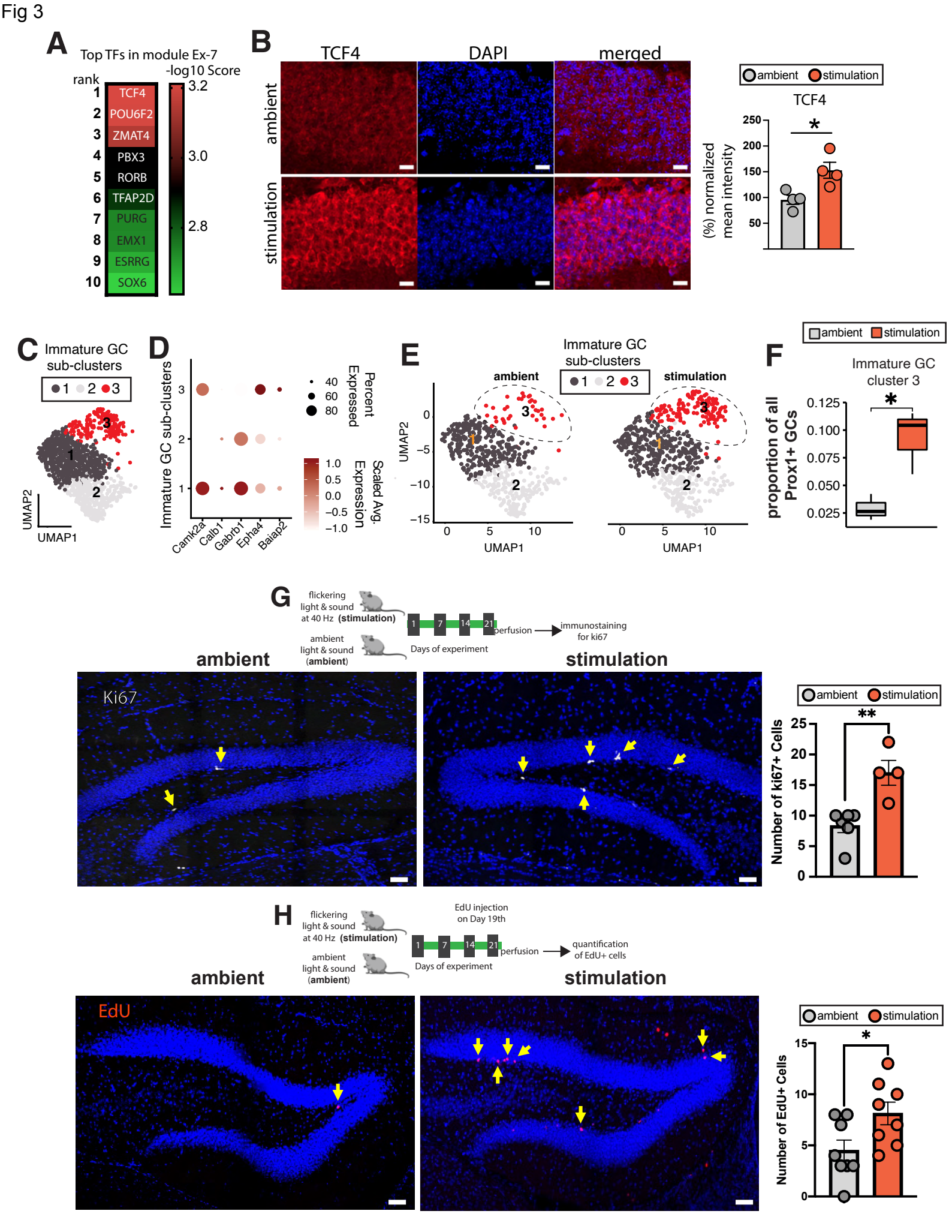
A
Top TFs in module Ex-7
rank
-log10 Score
1 TCF4
2 POU6F2
3 ZMAT4
4 PBX3
5 RORB
6 TFAP2D
7 PURG
8 EMX1
9 ESRRG
10 SOX6
3.2
3.0
2.8
B
TCF4
DAPI
merged
ambient
stimulation
ambient
stimulation
TCF4
(%) normalized mean intensity
250
200
150
100
50
*
C
Immature GC sub-clusters
1 2 3
UMAP2
UMAP1
D
Immature GC sub-clusters
Camk2a
Calb1
Gabrb1
Epha4
Baiap2
Percent Expressed
40
60
80
Scaled Avg. Expression
1.0
0.5
0.0
−0.5
−1.0
E
Immature GC sub-clusters
ambient
stimulation
1 2 3
UMAP2
UMAP1
F
ambient
stimulation
Immature GC cluster 3
proportion of all Prox1+ GCs
0.125
0.100
0.075
0.050
0.025
*
G
flickering light & sound at 40 Hz (stimulation)
ambient light & sound (ambient)
1
7
14
21
perfusion
immunostaining for ki67
Days of experiment
ambient
stimulation
Ki67
ambient
stimulation
Number of ki67+ Cells
25
20
15
10
5
0
**
H
flickering light & sound at 40 Hz (stimulation)
ambient light & sound (ambient)
EdU injection on Day 19th
1
7
14
21
perfusion
quantification of EdU+ cells
Days of experiment
ambient
stimulation
EdU
ambient
stimulation
Number of EdU+ Cells
15
10
5
0
*

Fig S1

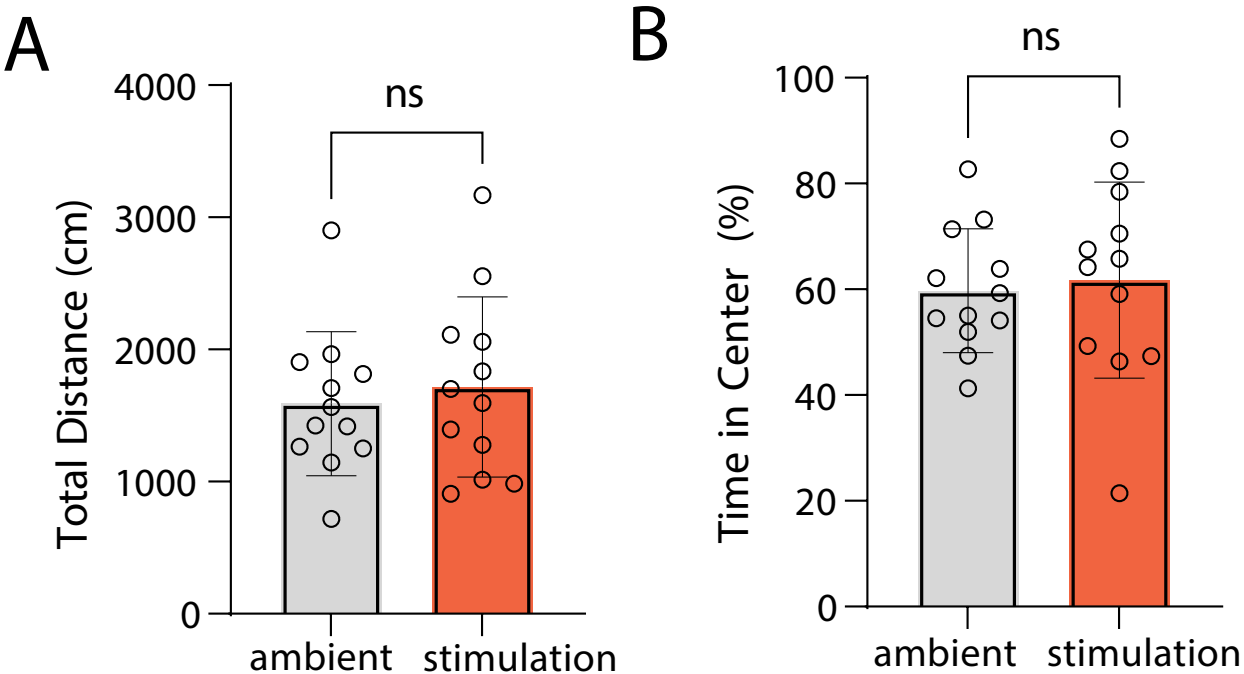
A
4000
3000
2000
1000
0
Total Distance (cm)
ns
ambient
stimulation
B
100
80
60
40
20
0
Time in Center (%)
ns
ambient
stimulation

Fig S2

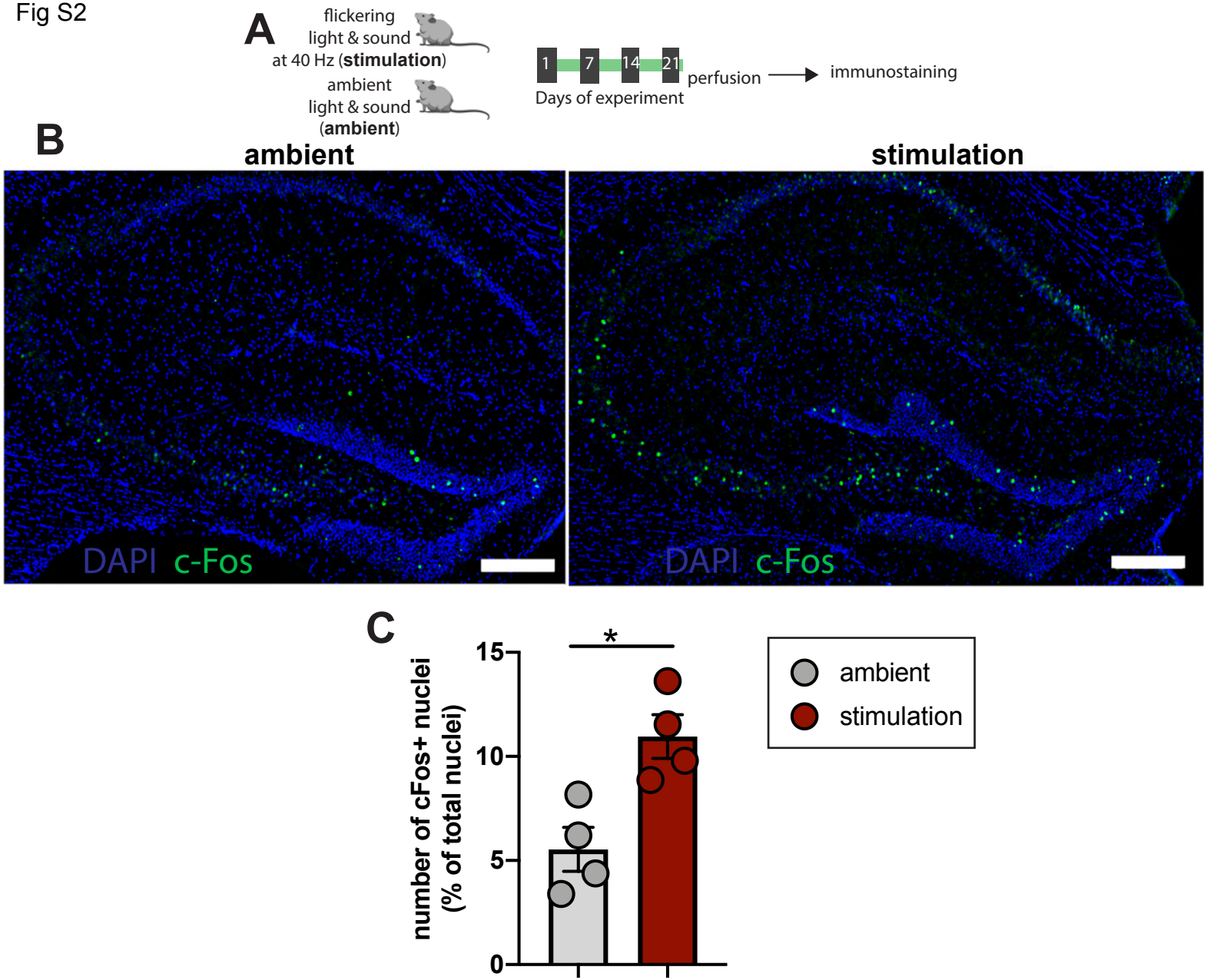
A
flickering
light & sound
at 40 Hz (stimulation)
ambient
light & sound
(ambient)
1
7
14
21
Days of experiment
perfusion
immunostaining
B
ambient
stimulation
DAPI c-Fos
DAPI c-Fos
C
number of cFos+ nuclei
(% of total nuclei)
15
10
5
0
*
ambient
stimulation

Fig S3

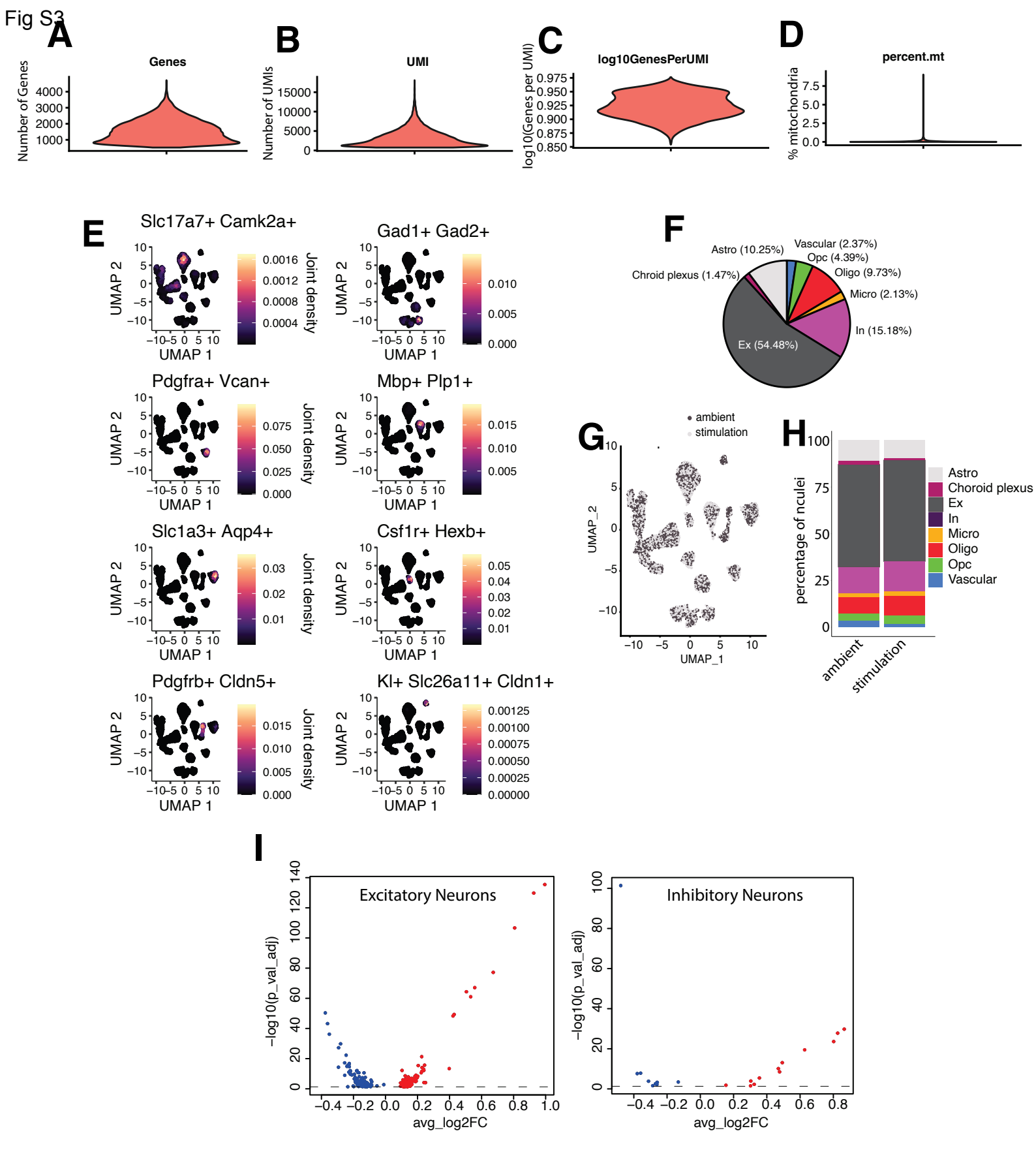
A
Genes
Number of Genes
4000
3000
2000
1000
B
UMI
Number of UMIs
15000
10000
5000
0
C
log10GenesPerUMI
log10(Genes per UMI)
0.975
0.950
0.925
0.900
0.875
0.850
D
percent.mt
% mitochondria
7.5
5.0
2.5
0.0
E
Slc17a7+ Camk2a+
Gad1+ Gad2+
Pdgfra+ Vcan+
Mbp+ Plp1+
Slc1a3+ Aqp4+
Csf1r+ Hexb+
Pdgfrb+ Cldn5+
Kl+ Slc26a11+ Cldn1+
UMAP 1
UMAP 2
Joint density
F
Astro (10.25%)
Vascular (2.37%)
Opc (4.39%)
Oligo (9.73%)
Micro (2.13%)
In (15.18%)
Ex (54.48%)
Chroid plexus (1.47%)
G
ambient
stimulation
UMAP_1
UMAP_2
H
percentage of nculei
Astro
Choroid plexus
Ex
In
Micro
Oligo
Opc
Vascular
ambient
stimulation
I
Excitatory Neurons
Inhibitory Neurons
−log10(p_val_adj)
avg_log2FC

Fig S4

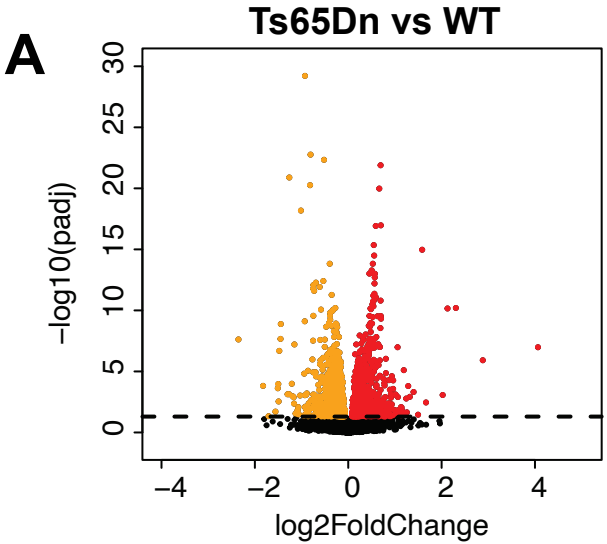
A
Ts65Dn vs WT
−log10(padj)
0
5
10
15
20
25
30
−4
−2
0
2
4
log2FoldChange

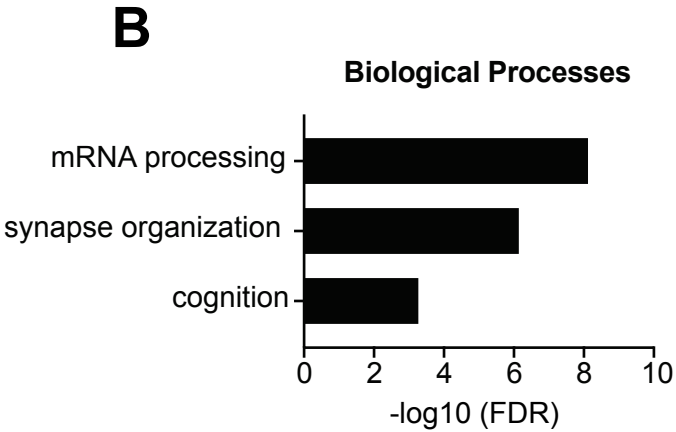
B
Biological Processes
mRNA processing
synapse organization
cognition
0
2
4
6
8
10
-log10 (FDR)

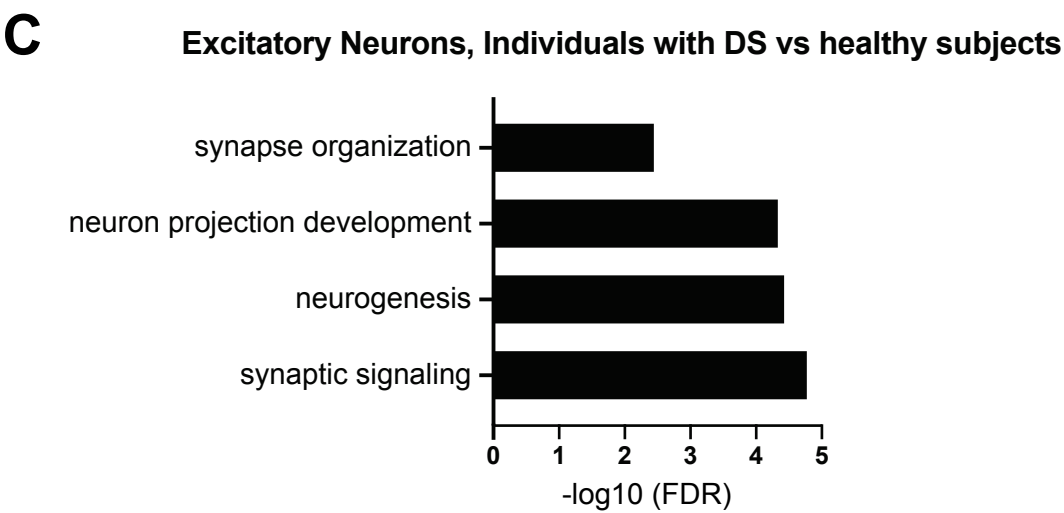
C
Excitatory Neurons, Individuals with DS vs healthy subjects
synapse organization
neuron projection development
neurogenesis
synaptic signaling
0
1
2
3
4
5
-log10 (FDR)

Fig S5

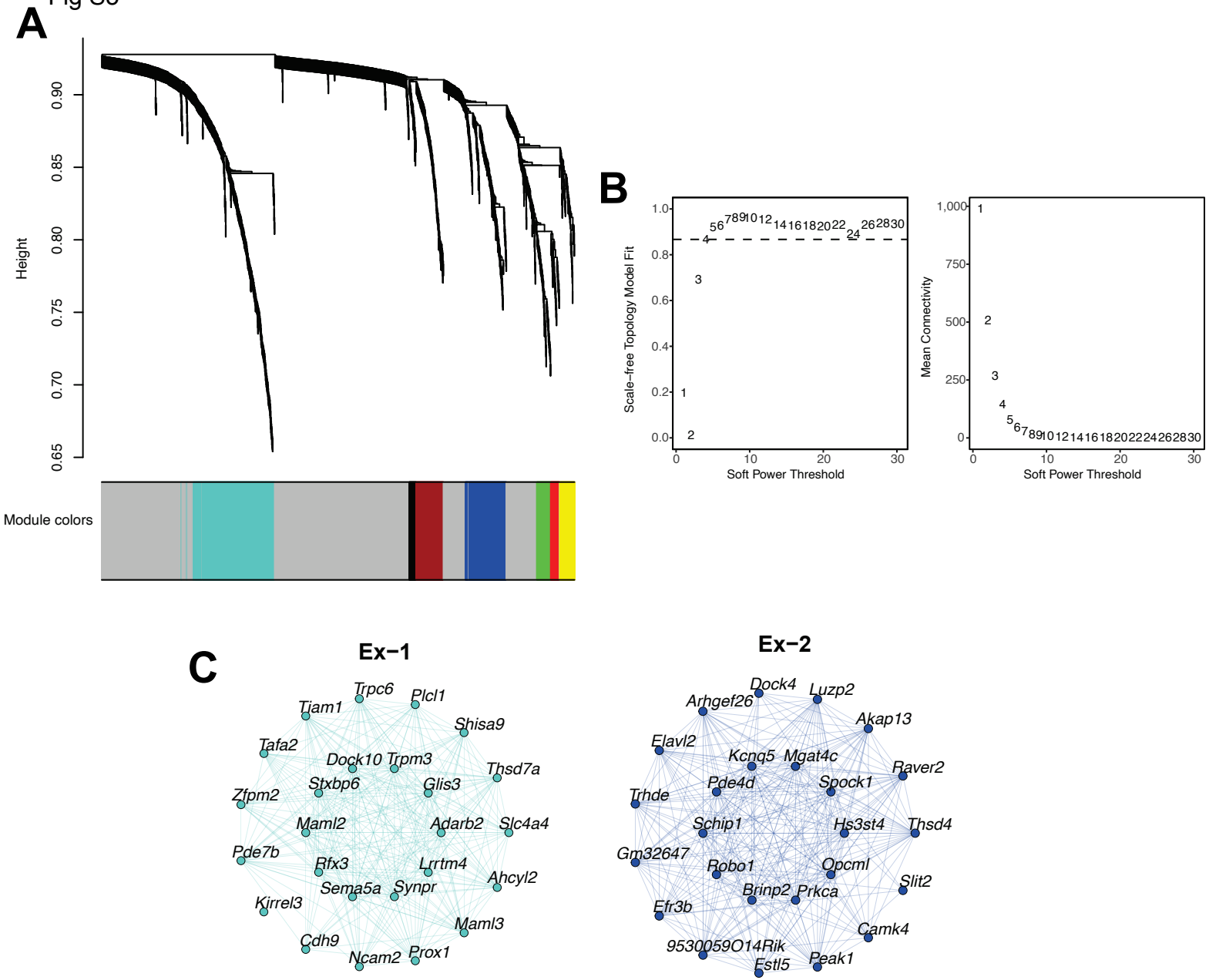
A
Height
0.65
0.70
0.75
0.80
0.85
0.90
Module colors
B
Scale−free Topology Model Fit
Soft Power Threshold
Mean Connectivity
Soft Power Threshold
C
Ex−1
Trpc6
Plcl1
Tiam1
Shisa9
Tafa2
Dock10
Trpm3
Thsd7a
Stxbp6
Glis3
Zfpm2
Maml2
Adarb2
Slc4a4
Pde7b
Rfx3
Lrrtm4
Ahcyl2
Sema5a
Synpr
Kirrel3
Maml3
Cdh9
Ncam2
Prox1
Ex−2
Dock4
Luzp2
Arhgef26
Akap13
Elavl2
Kcnq5
Mgat4c
Raver2
Pde4d
Spock1
Trhde
Schip1
Hs3st4
Thsd4
Gm32647
Robo1
Opcml
Slit2
Brinp2
Prkca
Efr3b
Camk4
9530059O14Rik
Peak1
Fstl5

Fig S6

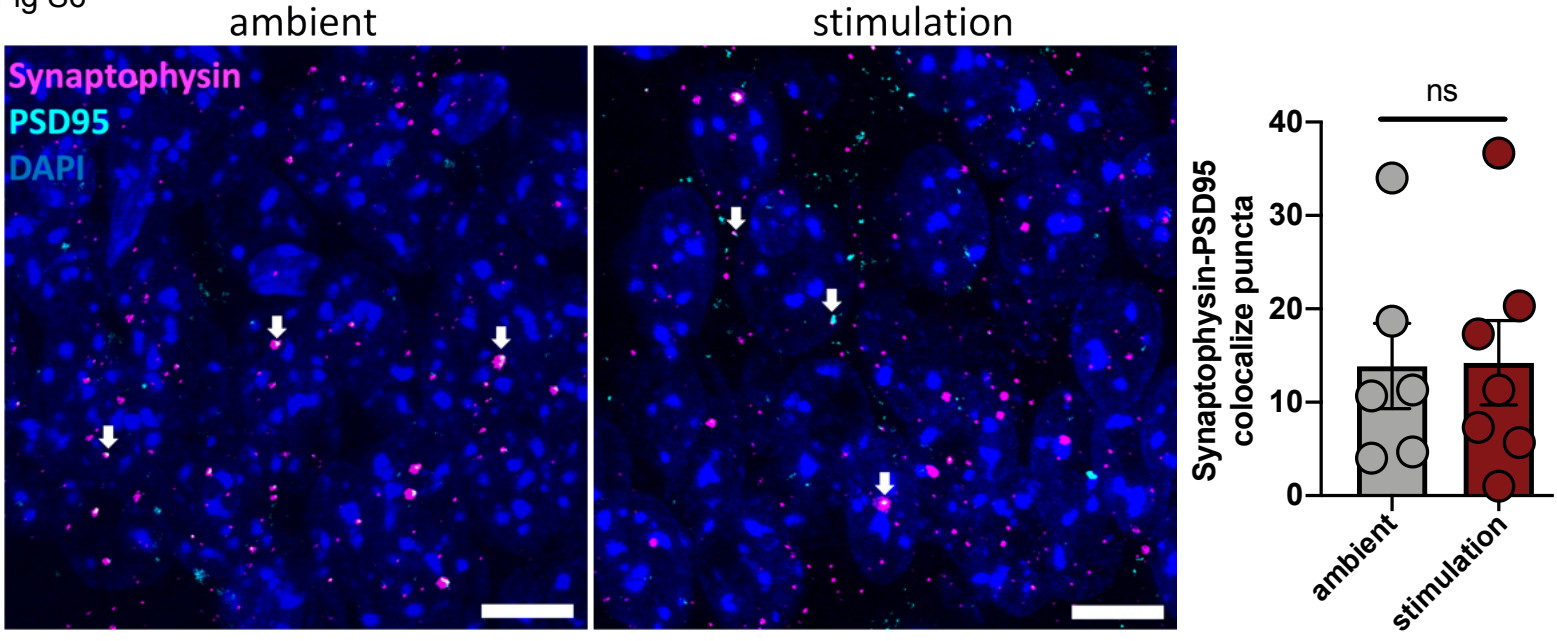
ambient
stimulation
Synaptophysin
PSD95
DAPI
ns
Synaptophysin-PSD95 colocalize puncta
40
30
20
10
0
ambient
stimulation

Fig S7

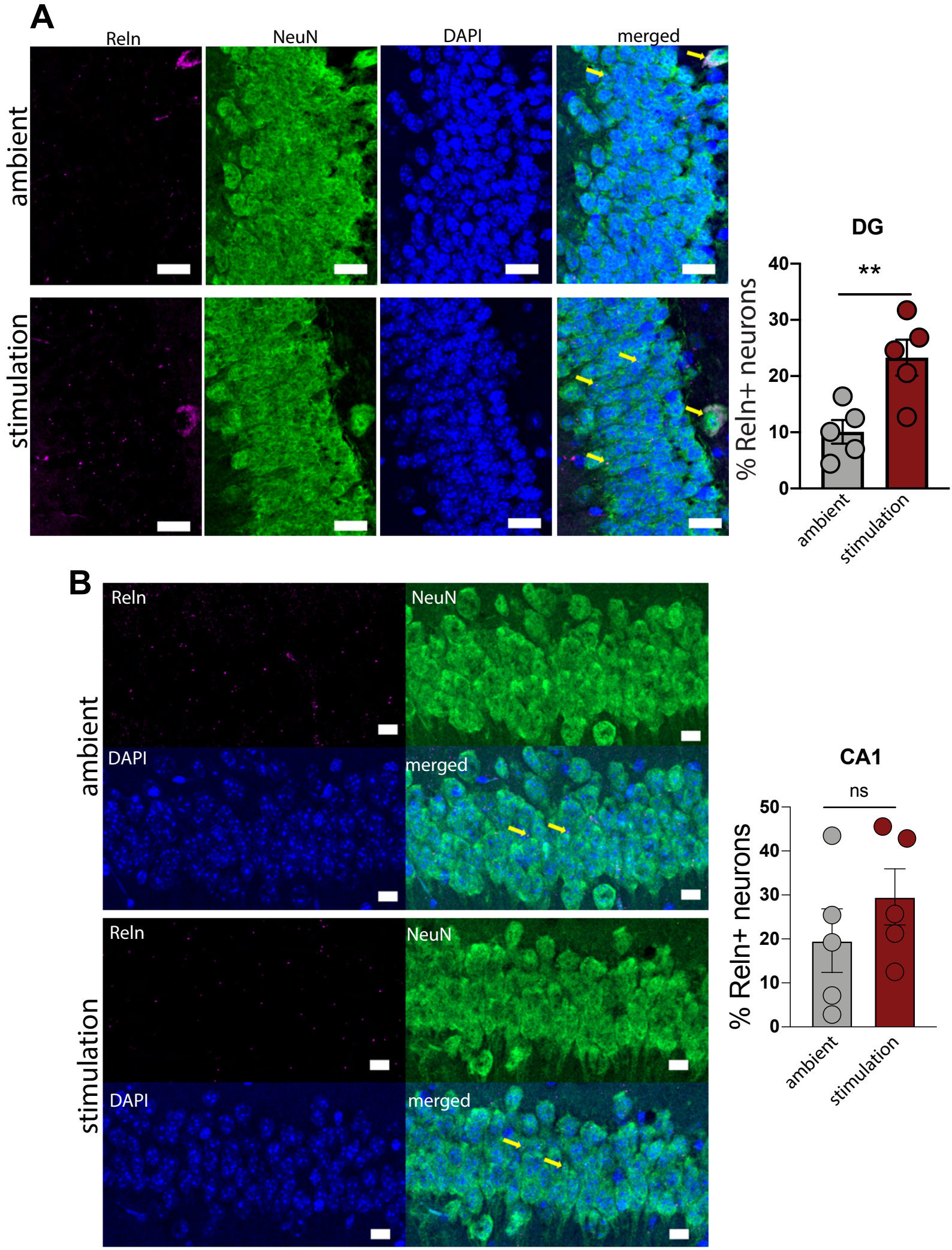
A
Reln
NeuN
DAPI
merged
ambient
stimulation
DG
**
% Reln+ neurons
40
30
20
10
0
ambient
stimulation
B
Reln
NeuN
DAPI
merged
ambient
stimulation
CA1
ns
% Reln+ neurons
50
40
30
20
10
0
ambient
stimulation

Fig S8

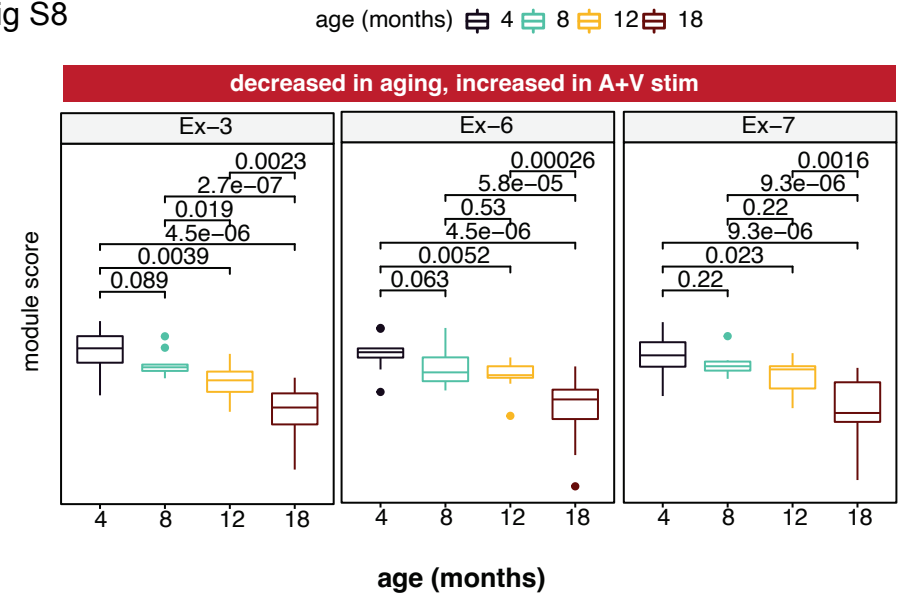
age (months) 4 8 12 18
decreased in aging, increased in A+V stim
Ex−3
Ex−6
Ex−7
0.0023
2.7e−07
0.019
4.5e−06
0.0039
0.089
0.00026
5.8e−05
0.53
4.5e−06
0.0052
0.063
0.0016
9.3e−06
0.22
9.3e−06
0.023
0.22
module score
4
8
12
18
age (months)

Fig S9

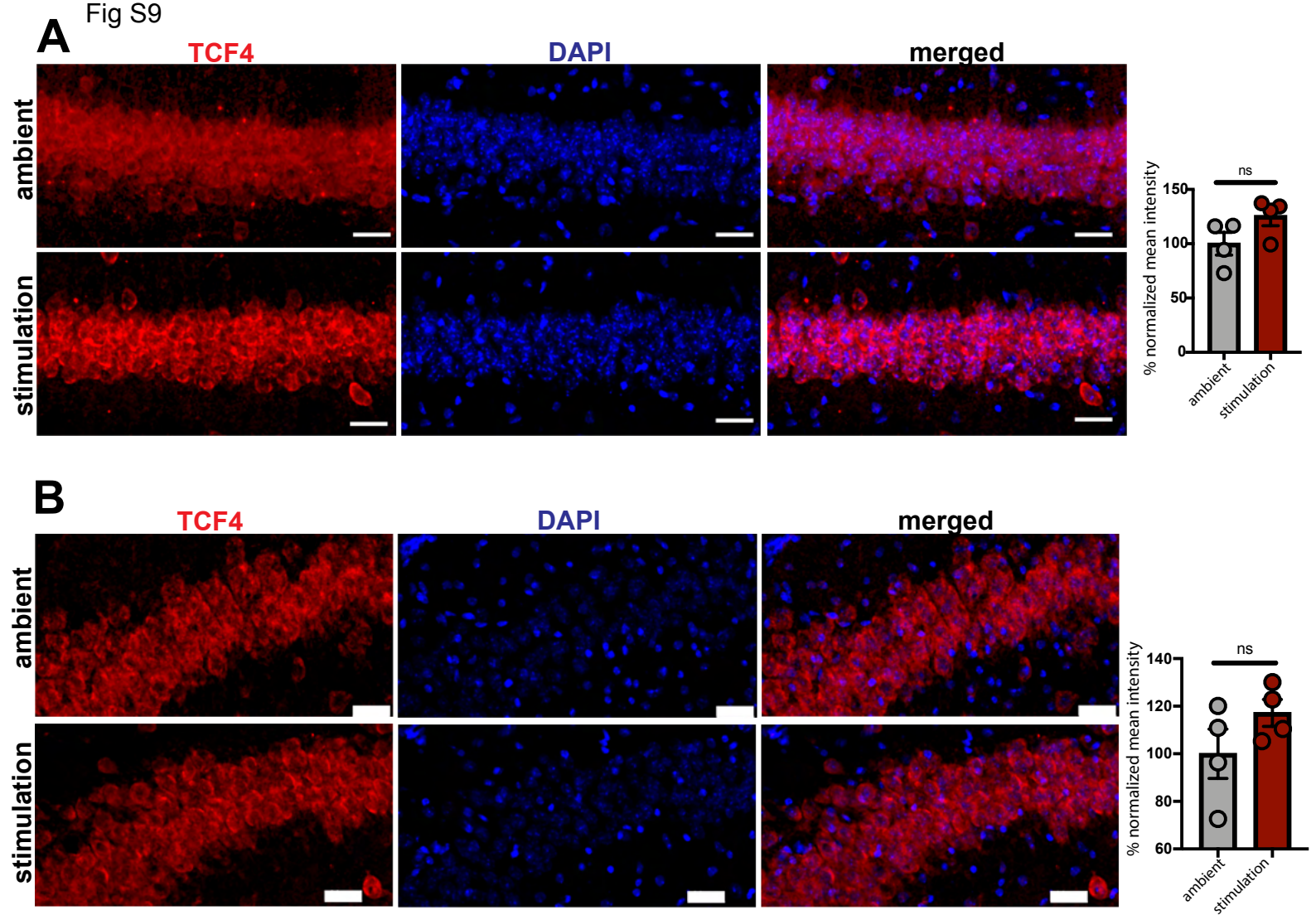
A
TCF4
DAPI
merged
ambient
stimulation
ns
% normalized mean intensity
150
100
50
0
ambient
stimulation
B
TCF4
DAPI
merged
ambient
stimulation
ns
% normalized mean intensity
140
120
100
80
60
ambient
stimulation

Fig S10

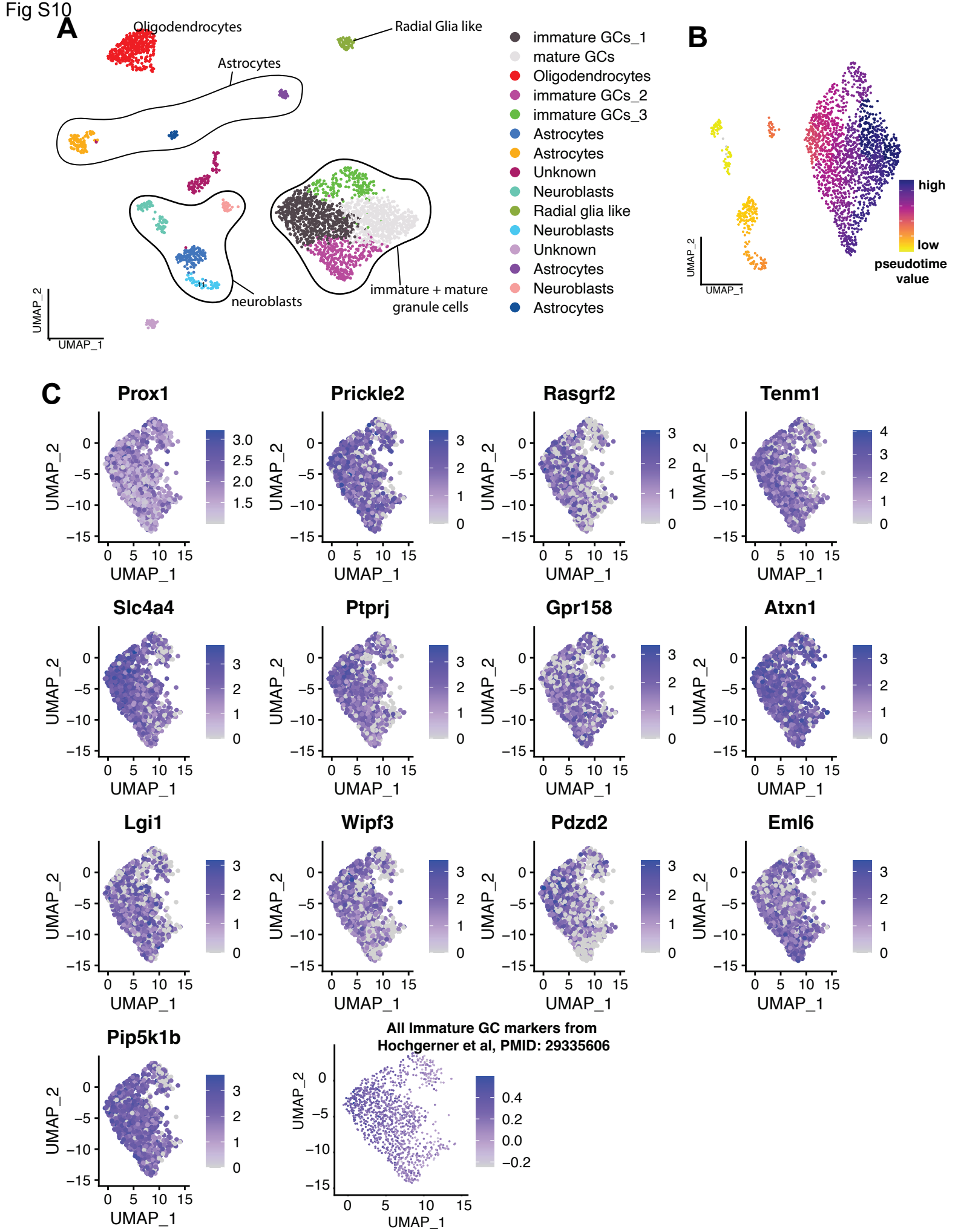
A
Oligodendrocytes
Radial Glia like
Astrocytes
neuroblasts
immature + mature granule cells
UMAP_2
UMAP_1
immature GCs_1
mature GCs
Oligodendrocytes
immature GCs_2
immature GCs_3
Astrocytes
Astrocytes
Unknown
Neuroblasts
Radial glia like
Neuroblasts
Unknown
Astrocytes
Neuroblasts
Astrocytes
B
high
low
pseudotime value
C
Prox1
Prickle2
Rasgrf2
Tenm1
Slc4a4
Ptprj
Gpr158
Atxn1
Lgi1
Wipf3
Pdzd2
Eml6
Pip5k1b
All Immature GC markers from Hochgerner et al, PMID: 29335606

Fig S11

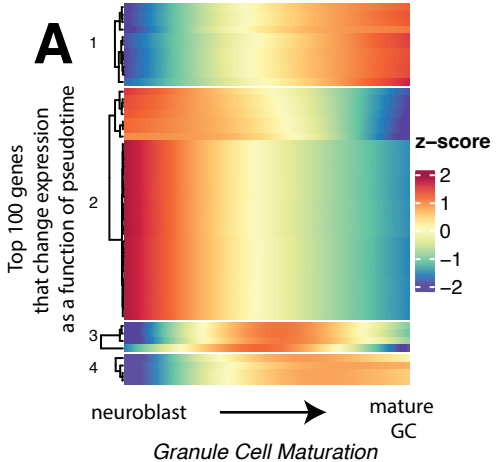
A
Top 100 genes
that change expression
as a function of pseudotime
1
2
3
4
z–score
2
1
0
−1
−2
neuroblast
mature
GC
Granule Cell Maturation

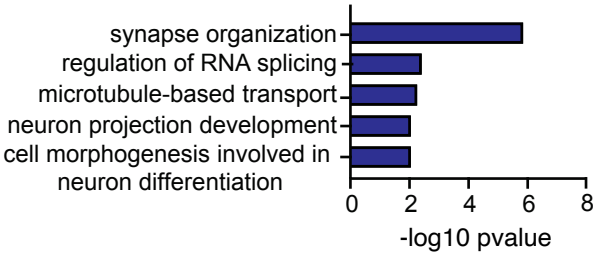
B
synapse organization
regulation of RNA splicing
microtubule-based transport
neuron projection development
cell morphogenesis involved in
neuron differentiation
0
2
4
6
8
-log10 pvalue

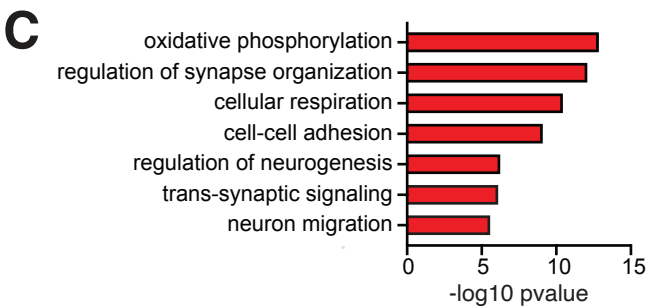
C
oxidative phosphorylation
regulation of synapse organization
cellular respiration
cell-cell adhesion
regulation of neurogenesis
trans-synaptic signaling
neuron migration
0
5
10
15
-log10 pvalue